
Sources and Levels of Background Noise in the NASA Ames 40- by 80-Foot Wind Tunnel—A Status Report

Paul T. Soderman, Ames Research Center, Moffett Field, California

May 1988



National Aeronautics and
Space Administration

Ames Research Center
Moffett Field, California 94035

SUMMARY

Background noise levels have been measured in the NASA Ames Research Center 40-by 80-Foot Wind Tunnel following installation of a sound-absorbent lining on the test-section walls. Results show that the fan-drive noise dominated the empty test-section background noise at airspeeds below 120 knots. Above 120 knots airspeed, the test-section broadband background noise was dominated by wind-induced dipole noise (except at lower harmonics of fan blade-passage tones) most likely generated at the microphone or microphone support strut. (Certain tones in the acoustic spectra were probably generated by the microphone support strut.) Third-octave band and narrow-band spectra are presented for several fan operating conditions and test-section airspeeds. The background noise levels compared well with published in-flow background noise from other wind tunnels. The data suggest that background noise levels can be reduced by making improvements to the microphone wind screen or support strut. Empirical equations are presented that relate variations of fan noise with fan speed or blade-pitch angle. An empirical expression for typical fan noise spectra is also presented. Fan motor electrical power consumption is related to the noise generation. Preliminary measurements of sound absorption by the test-section lining indicate that the 152-mm thick lining will adequately absorb test-section model noise at frequencies above 300 Hz.

NOMENCLATURE

D_H	fan hub diameter, m
D_t	fan tip diameter, m
F_n	number of fans in a system
f	frequency, Hz
l	characteristic dimension of vortex shedding body, m
$L_p(f)$	sound pressure level in frequency band with center frequency f , dB re 2×10^{-5} Pa
L_{pO}	overall sound pressure level, dB re 2×10^{-5} Pa
$L_w(f)$	sound power level in frequency band with center frequency f , dB re 10^{-12} Watt
M	Mach number of test-section flow
N	fan rotational speed, revolutions per minute (rpm)
St	Strouhal number
U	wind speed in test section, knots or m/s

U_{flow}	average axial airspeed through the fan section, m/s
U_{rot}	fan rotational tip speed, m/s
U_{tip}	resultant velocity at the fan tip, m/s
β	blade pitch angle between chord line and rotor disc measured at 3/4 radius, deg
$\Delta\beta$	change in fan blade pitch angle, deg
ΔdB	change in sound level, dB

INTRODUCTION

The NASA Ames Research Center 40- by 80-Foot Wind Tunnel (40 x 80) has been used for numerous aeroacoustic studies of aircraft models such as those described in references 1-3. Because of the recent installation of a 152-mm thick sound-absorbent lining on the test-section walls (refs. 4 and 5), the use of the facility for acoustic research will increase. Potential users of the facility require two key pieces of information to properly plan an aeroacoustic wind tunnel test: a) the anechoic properties of the test section, and b) the background noise of the test section. The first item will be touched on briefly and, it is hoped, will be the subject of a future acoustic calibration. The second item, the background noise, is the primary subject of this report.

A test was conducted to document the test-section noise floor, which is the minimum background noise of the test section with all struts and test hardware removed except for the microphone and its support strut. Data were acquired over a broad range of wind speeds and drive-fan operating conditions. In reality, the noise floor will change over time as modifications are made to the facility, and as improvements are made to the microphone nose cone and strut design. Thus, this is a status report on the continual effort to improve the acoustical characteristics of the wind tunnel. Results of our tests are compared with data from other wind tunnels in this country and abroad.

FACILITY, APPARATUS, AND INSTRUMENTATION

Wind-Tunnel Circuit

The Ames Research Center 40- by 80-Foot Wind Tunnel is a closed-circuit wind tunnel with a closed test section as shown in figure 1(a) and (b). The attached 80- by 120-Foot Wind Tunnel uses the same drive fans as the 40 x 80, but is sealed off when the 40 x 80 is operating. Six 40-ft diameter fans (driven by electric motors) are located in the drive section in two horizontal rows of three fans each as shown in figure 2(a) and (b). Table 1 lists the geometric and operating characteristics of a single fan. The variable-speed, variable-pitch fans can be operated from 0 to 180 rpm with blade-pitch angles from -18° to 52° relative to the fan disc. The maximum mass flow results in an airspeed of approximately 300 knots in the 40 x 80-ft test section. The wind tunnel performance is described in reference 6.

The 24-m long test section is connected to the settling chamber by an 8 to 1 area contraction. The test section has 12-m wide flat floor and ceiling sections, and semicircular walls that create a test section 12-m high and 24-m wide at the widest point (40 x 80 ft). Eight vortex generators are located near the diffuser entrance to stabilize the diffuser flow (ref. 7). The vortex generators are mounted in pairs as

shown in figure 3 so as to create vortex pairs of opposite rotation direction. Each flat-tip vortex generator is shaped like a 1.10-m span semispan wing mounted perpendicular to the duct wall. The airfoil sections are Clark-Y sections with 3.30-m chords. The angle of attack of each vortex generator is 15°. There is no screen or honeycomb in the circuit.

The test-section walls, exclusive of the floor, are lined with a 152-mm deep sound-absorbent lining composed of fiberglass bats wrapped in cloth and covered with a 40% open-area perforated steel plate as shown in figure 4(a) and (b). The floor lining is similar, but contains a 38-mm thick steel grating for support of personnel and equipment, that leaves a 114-mm thick fiberglass layer below the grating. The grating is supported every 0.6 m cross stream and every 3.0 m streamwise by structural members attached to the original floor. The lower half of each side wall contains an armor plating, portions of which are 16-mm or 32-mm thick, for personnel protection. The fiberglass lining is correspondingly thinner than 152 mm in those areas. The acoustic lining can be penetrated for attachment of struts and other hardware to the steel walls of the wind tunnel if necessary. Table 2 lists the relevant acoustic specifications of the lining. A significant part of the lining design is based on acoustic lining performance data and predictions made by Rennison et al. (ref. 8).

The sound absorption of the lining shown in figure 4(a) is fairly good above 300 Hz--as might be expected from a 152-mm thick lining. The absorption data were acquired by measuring impulsive sound reflected off 11-m² patches of the lining in the ARC 7- by 10-Foot Wind Tunnel as described in reference 5. Although a few pulse reflection measurements were made of the lining installed in the 40 x 80 that confirmed the patch-test results, detailed measurements have not been made of the test-section anechoic properties. Thus, local reflections from hinges, windows, corner vanes, vortex generators, or other hard points have not yet been identified. Nor have flow effects on the installed lining absorption been investigated. The patch-test measurements (ref. 5) showed a reduction of sound absorption with increasing airspeed; a reduction incorporated in the absorption curve in figure 4(a) for a nominal airspeed of 100 knots.

A 10.5-m diameter turntable covering a six-component balance system is located in the center of the test-section floor. Although a variety of mounting systems are available, a typical aircraft model would be mounted to three struts connected to the balance--two struts under the wing and one under the tail. The tail strut telescopes to vary aircraft angle of attack, and the turntable rotates to simulate aircraft yaw. The wing and tail struts are typically 6-m tall and are protected from the wind by fairings. These strut fairings are potential sources of wind-generated noise. A few acoustic spectra were obtained with two struts and fairings in place for comparison with the empty test-section data.

Microphones and Support Struts

The B&K 4133 - 13-mm (1/2 inch) diameter condenser microphone used for this study is robust and has a fairly uniform frequency response between 6 Hz and 15 kHz with the B&K bullet-shaped nose cone attached. The nose cone makes the microphone reasonably omnidirectional. To hold the microphone, a long slender tube was used. Glover and Shivashankara (ref. 9) showed that long slender microphone holders generated less wind noise than other bulkier designs.

The design of the microphone support strut is critical to minimizing the induced wind noise. Figure 5(a) and (b) show the tripod strut used for this study. The strut had a constant chord NACA 0015 airfoil cross section and was designed to be quite rigid in strong winds. This may have led to excess flow noise from the junction of the side braces and main strut, as will be discussed in the Results and Discussion section.

Generally, a tapered strut with a standard NACA airfoil shape such as NACA 0015 is preferred over a constant chord strut, but a tapered strut was not available for this study. A tapered strut has

strength low on the strut where the bending moments are highest, which minimizes vibrations, and has a small cross section near the microphone to minimize acoustic reflections. An NACA airfoil will minimize flow separation and vortex shedding that might otherwise occur on blunt oval tubing for example (ref. 10). However, in certain Reynolds number flow regimes, vortex shedding tones can still be generated on NACA airfoils (ref. 11), even with tapered struts, as demonstrated by Schlinker et al. (ref. 12). In that case, boundary-layer trips can be used to defeat the coherent vortex shedding. The trip can be as simple as sticky tape turned inside out and attached to the strut leading edge--a method used in this study in an attempt to eliminate certain tones in the acoustic spectra.

Figure 6 shows the two microphone stations used in the test section--stations #1 and #2. Most of the data were acquired at station #1, which was in the forward part of the test section just downstream of the acoustic-lining leading edge. To examine noise sources in the diffuser, the microphone and strut were moved downstream to station #2 during part of the study.

Instrumentation and Data Reduction

The microphone and preamp in the test section were connected to a power supply and amplifier in the control room adjacent to and below the test section. The data were recorded on an analog tape recorder. Selected channels were digitized and reduced on-line in the frequency domain. The bulk of the data were then digitized and reduced later from the analog recordings using a GR 1995 third-octave analyzer and an HP 3562A narrow-band spectrum analyzer. The narrow-band spectra were reduced to a 1-kHz, 10-kHz, 20-kHz, or 50-kHz maximum frequency range, which results in constant bandwidths of 1.25 Hz, 12.5 Hz, 25 Hz, and 62.5 Hz, respectively. A Hanning window was employed to minimize leakage during the FFT process. The broadband sound levels vary with bandwidth and, therefore, are not presented as true power spectral density (PSD). The broadband sound levels can be corrected to PSD by subtracting $10 \log \Delta f$ from the data plots, where Δf is the filter bandwidth for the particular frequency range. Tone levels are unaffected by filter bandwidth if they are 10 dB above the broadband level in the band. If tone levels are less than 10 dB above the broadband noise, the apparent tone level will be higher than would be represented in a PSD plot. Note that the data recorded 0-1 kHz are close to PSD data because the 1.25-Hz bandwidth is close to the 1.0-Hz bandwidth of PSD. Because of a DC bias in the narrow-band analyzer, the data below 10 Hz are not shown.

RESULTS AND DISCUSSION

Narrow-Band Spectra

When this study was initiated, there was a 13-m span by 0.6-m chord aerodynamic survey wing mounted on two struts in the test section, as shown in figures 4(b) and 7. The wing supported various probes for fluid-mechanic measurements (ref. 6). The survey apparatus generated flow-induced tones as shown in typical narrow-band noise spectra illustrated in figure 8, that were obtained with and without the survey apparatus installed. Assuming that the tones near 300 and 900 Hz are related to a vortex-shedding mechanism, a common noise source in wind tunnels (ref. 10), the shedding frequency is given by:

$$f = St U/l = 0.20 U/l \quad (1)$$

A Strouhal number of 0.20 was assumed based on the work of Schlinker et al. (ref. 12), who showed that the vortex-shedding tone from cylinders correlated well with that Strouhal number. For a frequency

of 300 Hz and an airspeed of 156 knots, equation (1) leads to a characteristic dimension, l , of the vortex-shedding body equal to 54 mm. That dimension corresponds to the cross-stream distance between vortex-shedding regions on the body, and is close to the support strut tip extension diameter of 62 mm. (A Strouhal number of 0.23 would have given perfect agreement between the predicted and measured body dimension.) Hence, the exposed 203-mm long cylindrical strut tips supporting the survey wing are the likely source of the tone at 300 Hz. The survey wing itself, which had a 51-mm thick truncated trailing edge, was also suspected to be a vortex shedding body. However, the wing chord-based Reynolds number of 3.3×10^6 is beyond the range of coherent vortex shedding of conventional airfoils according to the work of Paterson et al. (ref. 13) (unless the truncation forces vortex shedding at high Reynolds number). Similar arguments hold for the various strut fairings. The tone near 900 Hz was probably a harmonic of the 300 Hz tone, since no component on the survey rig was identified with the appropriate dimension (18 mm) for that tone based on equation (1). No attempts were made to eliminate the vortex shedding from the support struts.

The empty test-section (survey wing and struts removed) background noise data for a range of airspeeds are given in figure 9(a)-(h). The data were measured at the forward microphone station #1. Narrow-band data from 10 to 20 kHz are presented to illustrate the details of the background noise. More conventional third-octave band data will be presented later. The spectra are similar to each other in that all the curves are maximum at the low-frequency end of the spectra because of the fan-drive noise, followed by a gradual decrease in broadband noise as frequency increases. Figure 10(a)-(i) illustrate background noise data analyzed from 10 to 1 kHz to highlight the low-frequency noise. The blade-passage frequency of the fan noise is 45 Hz for 180 rpm fan speed, with harmonics at multiples of 45 Hz, which can be identified out to the third or fourth harmonic in figure 10(e). These tones appear to dominate the test-section low-frequency noise at most airspeeds and fan operating conditions.

Tones not related to the fan drive were also generated. Figure 9(b), for example, shows a tone at 4500 Hz (at 54 knots airspeed), which projects about 14 dB above the broadband noise. Using equation (1), the estimated body dimension responsible for vortex shedding at that frequency would be 1.2 mm. There were no wires in the airstream anywhere in the test section. No cavities or cracks in the test-section walls could be found generating tones. There were small protuberances such as bolt studs at various places on the walls, but such small aerodynamic bodies would probably be incapable of creating a strong tone unless the disturbance was very close to the microphone. It is suspected that the tone came from the microphone strut; possibly at the junction of the two support struts and main strut shown in figure 5(b). Data taken in the same test section five years ago with the same type microphone and nose cone, but with a different strut geometry, did not exhibit this particular tone. In any case, the data are presented as measured--all tones included.

As airspeed increased, the strut tone frequency increased as predicted by equation (1) until an airspeed of 136 knots was reached--at which point the tone disappeared. Since coherent aerodynamic disturbances are Reynolds-number sensitive, it is likely that the higher Reynolds number flow caused the coherent structure of the disturbance to break down into a random flow. At 136 knots, the chord-based Reynolds number of the strut was 9.27×10^5 . It should be noted that attempts were made to eliminate the tone by tripping the boundary layer at the strut leading edges, and to fill in all screw heads and other protuberances on the strut and microphone holder with wax--all without success. Thus, the strut junction is a likely candidate for the tone generation since the complex flow in that region is fairly insensitive to surface smoothness. In retrospect, that junction could have been aerodynamically cleaner by reducing the size of the side braces at the junction, and by locating the junction farther from the microphone.

Figure 9(e) shows that a strong tone developed at 19.5 kHz and 148 knots airspeed that was unrelated to the strut tone discussed above. Glover and Shivashankara (ref. 9) discovered similar tones near this airspeed while also using a B&K microphone and nose cone. They attributed the tones to microphone self noise, presumably (we suppose) caused by cavity resonance. They found that the tones varied from nose cone to nose cone and also changed unpredictably because of changes in flow conditions. The tones

were often attenuated by other noise sources. Thus, data falling near these resonance frequencies would be suspect.

During one series of tests, the microphone was moved downstream near the diffuser inlet to investigate possible noise from the diffuser vortex generators. Figure 11 is a comparison of acoustic spectra measured upstream (station #1) and downstream (station #2) of the test section center at 117 knots airspeed. The data indicate that the noise is slightly greater at the downstream station in the frequency range 10 to 4 kHz. Furthermore, there are variations in the tone levels around 10-12 kHz, the tones previously identified as coming from the microphone strut junction. Although the fact that the tones changed when the microphone was moved closer to the diffuser suggests that the diffuser might be the source of the tones, a close examination of the data does not show a consistent trend; some tone levels increased, some decreased. Thus, the tones could very well have come from the microphone strut, which may have been slightly rotated relative to the free stream during the relocation from station #1 to station #2. A rotation would have changed the strut angle of attack, which would have affected the relative tone amplitudes.

It is clear, however, that the low-frequency noise in figure 11, from 10 to 4 kHz, increased because of the microphone relocation and, therefore, did not come from the microphone strut. This data indicated that the low-frequency noise increase at the downstream station came either from the vortex generators or from the fan drive as an upstream propagation. However, the vortex generators can be ruled out since other data (discussed in the next section) show that the drive fans are the dominant noise source at this airspeed. Furthermore, fan noise propagation upstream into the test section is the dominant acoustic path because vane set 6, the first corner vane set downstream of the fan drive, is the only vane set in the 40 x 80 circuit that is acoustically treated (see fig. 12) and thereby attenuates fan noise propagating downstream. (The noise reduction of that vane set is shown in figure 13.) Since the upstream sound propagation will attenuate somewhat as it passes through the acoustically treated test section, the downstream microphone (station #2) should record higher fan-noise levels than the upstream microphone (station #1).

Third-Octave Band Spectra

To compare the 40- by 80-Foot Wind Tunnel background noise with that from other wind tunnels (as is done in the following section titled Comparison With Other Wind Tunnels), it is necessary to present the data in third-octave bands. Therefore, figure 14(a)-(h) illustrate the same empty test-section data of figure 9(a)-(h), but plotted in third-octave bands. The same trends observed in the narrow-band data are apparent in the third-octave bands, but the tonal resolution is poor in the third-octave band plots.

By comparing noise levels measured in the test section with noise levels measured in the west leg between the fan drive and the first downstream corner, it is possible to draw some conclusions about the sources of background noise. Figure 15(a)-(d) show west-leg noise variations with test-section airspeed for three fan speeds: 90, 135, and 180 rpm. Overall noise levels and selected third-octave band levels are presented. Also listed on the curves is fan blade-pitch angle, which is the angle between the blade chord line and rotor plane at the 3/4 radius station. Note that at low speeds, it is possible to achieve a 10-20 dB noise reduction in the west leg at a given airspeed by operating the fans at low rpm and high blade pitch. This trade-off is discussed in detail in reference 14. To achieve airspeeds above 150 knots, the fan must be operated at the top speed of 180 rpm.

The variation of test-section background noise with airspeed plotted in figure 16(a)-(d) have similar trends to the noise in the west leg (figure 15(a)-(d)), but with two important exceptions. First, the difference between the low- and high-rpm noise in the test section is much smaller than was measured in the west leg. The curves tend to merge such that, as the airspeed approaches 120 knots, the test-section noise becomes independent of fan speed and depends solely on wind speed. Second, the noise in the test section increases with airspeed at a different rate than it does in the west leg. This latter point is shown more clearly in figure 17, which compares the west-leg and test-section noise for 180 rpm fan operation.

(The 800 Hz third-octave data are representative of spectral trends except for low-frequency blade-passage tones.) Although the west-leg noise is greater than test-section noise at low airspeeds, the test-section noise is stronger at speeds above 120 knots. Thus, we can conclude that the fan-drive noise dominates the test-section background noise below 120 knots airspeed, but some other noise source dominates at speeds above 120 knots, except at very low frequencies. The rate at which the test-section noise increases with airspeed indicates that the noise source is a wind-induced dipole in the test section or at the microphone itself. This will be clear by considering the three noise variations in the wind tunnel : a) the variation of fan noise with blade pitch (fixed fan speed), b) the variation of fan noise with fan speed (fixed pitch), and c) the variation of test-section noise with airspeed.

Fan Noise vs Blade Pitch- To understand the fan noise characteristics, it is helpful to plot the fan sound power. The fan sound power was determined from the west-leg acoustic data by comparing the fan-drive sound levels with those generated by a calibrated noise source in the fan section (ref. 14). Figure 18 shows the fan sound power variation with airspeed on a semi-log scale. The maximum sound power was approximately 155 dB re 10^{-12} Watts. The solid lines in figure 18 correspond to fan operation at fixed rotational speed and variable pitch (pitch angles are noted above the data points); the dashed lines correspond to fan operation at fixed blade pitch and variable rotational speed. The operation at 90 and 135 rpm was stopped at a blade angle of 24° because of high current in the motor generator set. (The fans were not near stall.) It is estimated that the envelope could be expanded to approximately 30° blade angle at 90 and 135 rpm without modifications to the motors. Further expansion of the envelope at low rpm would require substantial modifications to the motor generator set. The variation of fan noise with blade pitch (fixed rpm) over much of the fan operating range is:

$$\begin{aligned} \Delta\text{dB} &= 0.3 \Delta\beta && \text{for } 16^\circ \leq \beta < 38^\circ \\ \Delta\text{dB} &= 0.5 \Delta\beta && \text{for } 38^\circ \leq \beta < 48^\circ \end{aligned} \quad (2)$$

where $\Delta\beta$ is the change in blade pitch angle in degrees. This is a weaker noise variation than the variation with fan speed except near top speed where the tip is approaching stall. The weak effect of blade pitch is related to the fan design and resulting efficiency (ref. 14). The fan was designed with a high twist so that the blade would have fairly uniform span loading at the maximum blade pitch angle of 52° and 180 rpm (top test section speed of 300 knots). At low blade pitch, the tip is lightly loaded and slowly approaches the design load as pitch is increased. The fan efficiency versus mass flow curve is fairly flat. The fan noise, therefore, varies slowly with blade pitch as well. If blade pitch is increased to the point where tip stall commences, the noise will increase sharply. It should be noted that equation (2) is an empirical equation that may not be valid for all fans since the noise is caused by steady and unsteady blade loading, which depends not only on blade pitch but also on the details of fan design and flow conditions.

Fan noise vs fan rotational speed- The fan noise variation with rotational speed (fixed blade pitch) from condition 1 to condition 2, based on the data in figure 18, is given by:

$$\Delta\text{dB} = 10 \log (N_2/N_1)^{5.2} \quad (3)$$

Equation (3) is typical for fan noise, though exponents varying from 5.0 to 6.0 are often reported, and is indicative of dipole sources on the blades. However, the test-section noise variation with airspeed is somewhat different than either equations (2) or (3) as illustrated by figure 17.

Test-section noise vs airspeed- Figure 17 shows that the test-section noise above 120 knots (excluding very low frequencies) increased faster with airspeed than the fan noise did. By plotting the test-section data on a semi-log plot (not shown), it was found that the noise varied approximately as:

$$\Delta dB = 10 \log (U_2/U_1)^6 \quad (4)$$

Thus, the test-section noise is created by dipole sources, which is a well-known acoustic source created by solid bodies in a moving stream. There are two reasons why the test-section noise increases faster than the fan noise above 120 knots airspeed: 1) in that regime, the fan is operated with fixed rotational speed and the fan noise variation with blade pitch (equation (2)) is weak, as discussed above, and 2) the airspeed changes much faster in the test section than at the fan blade. Above 120 knots, the fan is operated at a fixed 180 rpm and variable blade pitch. The resultant velocity (U_{tip}) at the fan blade tip, the region of greatest noise generation, is given by:

$$U_{tip} = (U_{rot}^2 + U_{flow}^2)^{0.5} \quad (5)$$

where U_{rot} is the rotational speed modified by induced swirl and U_{flow} is the axial airspeed. At 180 rpm, $U_{rot} = 105$ m/s, which is greater than the airspeed component. (The average value of U_{flow} is 71 m/s at the top speed of the wind tunnel.) Thus, a large increase in test-section speed is associated with a small increase in the resultant velocity at the blade tip. Equation (5) can be used to show that a doubling of the test-section airspeed only requires a 10% increase in U_{tip} during fixed rpm operation of the fan. Thus, the unsteady fan blade loading, which changes because of blade pitch and flow speed, increases slower than the test section dipole sources at test-section airspeeds over 120 knots.

Fan electrical and acoustical power- It is interesting and logical that the fan operating condition for minimum noise is also the condition for minimum electrical power consumption. Listed on figure 18 are the electrical power consumptions of the drive motors in Mega Watts (MW) for the various operating conditions. At 75 knots airspeed, the 90 rpm operation required 4 MW, while the 180 rpm operation at the same airspeed required 7 MW. Obviously, the noisy condition is also an aerodynamically and mechanically inefficient operation. Another way to look at this is to consider acoustic efficiency, which is the acoustic power divided by the electrical power consumed. Using the data from figure 18 plotted in terms of acoustic efficiency, figure 19 shows that the fan is a more efficient noise source at high rpm than at low rpm. (Of course, we want low acoustic efficiency in this case.) Consider the 180 rpm curve. The high level at 25 knots airspeed is caused by partial blade stall at 0° blade pitch. As blade pitch is increased, the acoustic efficiency drops to a more-or-less constant value until the blade pitch reaches a sufficient angle such that the blade tip loading, steady and unsteady, becomes substantial. Under these conditions, the noise and acoustic efficiency rise. The large region of uniform acoustic efficiency is consistent with the fairly uniform aerodynamic efficiency of the fans in the same operating range. The low acoustic efficiency at low rotational speed is due to the strong dependence of fan loading noise, both steady and unsteady, on tip speed.

The fan sound power levels were determined experimentally. In reference 14, it was shown that fan sound power can be predicted with an empirical equation based on compilations of data from many fans. The sound power in a third-octave band is given by:

$$L_w(f) = -58.2 - 10 \log [1 + (4.4 Qf/N)^2] + 10 \log f + 40 \log N + 70 \log D_t \\ + 10 \log Q + 10 \log F_n + 0.3 \beta \quad (\text{dB re } 10^{-12} \text{ Watt}) \quad (6)$$

where $Q = 1 - (D_H / D_t)^3$. Equation (6) is valid for fan dimensions in meters. The overall sound power level is found by summing the acoustic power (Watts) in the third-octave bands. Figure 20 is a comparison of the measured fan third-octave sound power spectrum and the predicted spectrum from equation (6). The spectrum shape indicates that both steady and unsteady loading noise sources were present.

Comparison With Other Wind Tunnels

Figure 21(a) and (b) show noise levels from the 40-by 80-Foot Wind Tunnel compared with published data from four other wind tunnels--the DNW Wind Tunnel in Holland (ref. 9), the Langley 14- by 22-Foot Wind Tunnel (ref. 15), the Ames 7- by 10-Foot Wind Tunnel No. 1 (ref. 16), and the RAE 1.5 m Wind Tunnel (ref. 17). These wind tunnels were chosen because they are used for aeroacoustic research; many others could have been included. In-flow microphone noise in the 800 and 2500 Hz third-octave bands is shown. The data show a remarkable similarity. With the exception of the Langley 14- by 22-Foot Wind Tunnel data at 800 Hz, all the data tend to have similar magnitudes and a similar variation with airspeed. Hence, most of the data follow a V^6 variation indicative of wind-induced dipole noise. The Langley wind-tunnel noise is dominated by fan noise, which is aggravated by inefficient fan performance possibly caused by tip stall (ref. 15). (Yu and Abrahamson, ref. 18, have proposed a scheme to rebuild the fan and thereby reduce the noise in the 14 x 22-ft test section substantially.) Since most of the data are similar to the 40 x 80 background noise, and since the 40 x 80 background noise above 120 knots has been traced to wind-induced noise in the test section, it follows that the mid- to high-frequency background noise above 120 knots from the other wind tunnels (except the Langley 14 x 22) is probably dominated by wind noise and not by fan-drive noise or other sources (exclusive of lower harmonics of blade-passage noise.) Furthermore, since some of the data were taken in open-jet wind tunnels and some in closed-jet wind tunnels, boundary-layer noise on the test-section walls is not the source, which leaves the microphone and/or microphone strut as the likely source. (Boundary-layer noise is quadrupole in nature, in any case.) Struts are especially good noise sources when they span open-jet shear layers. Thus, the noise floor of many current facilities may be controlled by the current technology in microphones, nose cones, and support struts. Since the 40 x 80 noise is slightly louder than the other wind-tunnel data, improvements in the microphone support strut used in this study should result in modest reductions in background noise. Further gains will have to await improvements at the microphone itself.

CONCLUSIONS

Measurements of background noise in the NASA Ames 40-by 80-Foot Wind Tunnel have shown that the fan-drive noise dominated the empty test-section background noise at airspeeds below 120 knots. Above 120 knots the test-section background noise was dominated by wind-induced dipole noise (except at lower harmonics of fan blade-passage tones) most likely generated at the microphone or microphone support strut. Typical third-octave noise levels were between 85 and 95 dB for an airspeed of 148 knots. Above 120-knots airspeed, the noise varied approximately as airspeed to the 6th power. Below 120 knots, the noise depended on fan operating mode. Variable fan speed operation, fixed pitch, caused the noise to vary as fan speed to the 5th power. Variable pitch operation, fixed rpm, caused a noise variation $\Delta dB = 0.3 \Delta\beta$ to $0.5 \Delta\beta$, where $\Delta\beta$ was the blade pitch change. Certain mid-frequency tones in the acoustic spectra were probably generated by the microphone support strut. High-frequency tones were suspected to come from the microphone noise cone. Fan motor electrical power consumption had the same trends with operating condition that the noise generation did; that is, high fan tip speed generated both high noise and high power consumption. An empirical expression for typical fan noise is presented in equation (6).

The background noise levels compare well with in-flow background noise from other aeroacoustic wind tunnels. In fact, the noise comparisons suggest that a number of wind tunnels used for acoustic research in this country and abroad have similar in-flow background noise levels dominated by wind-induced noise near the microphone. The data presented here represent the current noise floor of the test section with a microphone support strut installed. The background noise levels above 120 knots could probably be reduced by: 1) improvements to the support strut, 2) improvements to the microphone wind screen, and 3) expansion of the low rpm operating regime of the fan drive. Future work will concentrate on items (1) and (3). The background noise levels below 120 knots could probably be reduced by acous-

tically treating certain corners in the circuit (see ref. 16) or by operating the fans at lower rotational speeds than were used in this study.

Preliminary measurements of sound absorption by the test-section lining indicate that the 152-mm thick lining will adequately absorb test-section model noise at frequencies above 300 Hz.

REFERENCES

1. Atencio, A. A.; and Soderman, P. T.: Comparison Of Aircraft Noise Measured In Flight and in the NASA Ames 40-by 80-Foot Wind Tunnel. AIAA Paper 73-1047, Oct. 1973.
2. Falarski, M. D.; Koenig, D. G.; and Soderman, P. T.: Aspects Of Investigating STOL Noise Using Large-Scale Wind-Tunnel Models. Canadian Aeronautics and Space Journal, vol. 19, no. 2, Feb. 1973.
3. Ahtye, W. F.; Miller, W. R.; and Meecham, W. C.: Wing and Flap Noise Measured by Near- and Far-Field Cross-Correlation Techniques. AIAA Paper 79-0667, March 1979.
4. Soderman, P. T.: A Comparison Of Wind Tunnels Suitable For Rotorcraft Noise Studies. NASA CP 2234 - Rotorcraft Noise, 1982, pp. 45-62.
5. Soderman, P. T.: Oblique Incidence Sound Absorption of Porous Materials Covered by Perforated Metal and Exposed to Tangential Airflow. Inter-noise 82, Proceedings of International Conference on Noise Control Engineering, vol. 11, May 1982, pp. 401-404.
6. Olson, L. E.; Zell, P. T.; Soderman, P. T.; Falarski, M. D.; Corsiglia, V. R.; and Edenborough, H. K.: Aerodynamic Flow Quality and Acoustic Characteristics of the 40- by 80-Foot Test-Section Circuit of the National Full-Scale Aerodynamic Complex. SAE Tech Paper 872328, Dec. 1987.
7. Schmidt, G. I.; Rossow, V. J.; Van Aken, J.; and Parrish, C. L.: One-Fiftieth Scale Model of 40- by 80-Foot and 80- by 120-Foot Wind Tunnel Complex at NASA Ames Research Center. NASA TM 89405, April, 1987.
8. Rennison, D. C.; Wilby, J. F.; and Gordon, C. G.: Design Concepts For Sound Absorbing Linings in the Test Section of the NASA Ames 80 x 120 Foot Wind Tunnel. NASA CR-152155, May 1978.
9. Glover, B. M.; and Shivashankara, B. N.: Aeroacoustic Testing in Wind Tunnels. AIAA Paper 86-1886, July 1986.
10. Soderman, P. T.: Test-Section Noise of the Ames 7-by 10-Foot Wind Tunnel No. 1. NASA TM X-73,134, May 1976.
11. Hersh, A. S.; Soderman, P. T.; and Hayden, R. E.: Investigation of Acoustic Effects of Leading-Edge Serrations on Airfoils. J. of Aircraft, vol. 11, no. 4, April 1974, pp. 197-202.
12. Schlinker, R. H.; Fink, M. R.; and Amiet, R. K.: Vortex Noise from Nonrotating Cylinders and Airfoils. AIAA Paper 76-81, Jan. 1976.
13. Paterson, R. W.; Vogt, P. G.; Fink, M. R.; and Munch, C. L.: Vortex Noise of Isolated Airfoils. J. Aircraft, vol. 10, no. 5, May 1973, pp. 296-302.
14. Soderman, P. T.; and Mort, K. W.: Aeroacoustic Characteristics of a Large, Variable-Pitch, Variable-Speed Fan System. Inter-Noise 83 Proceedings (International Institute of Noise Control Engineering), vol. 1, Edinburgh, July, 1983, pp.123-126.
15. Hayden, R. E.; and Wilby, J. F.: Sources, Paths, and Concepts for Reduction of Noise in the Test Section of the NASA Langley 4 x 7m Wind Tunnel. NASA CR 172446-1, Sept. 1984.

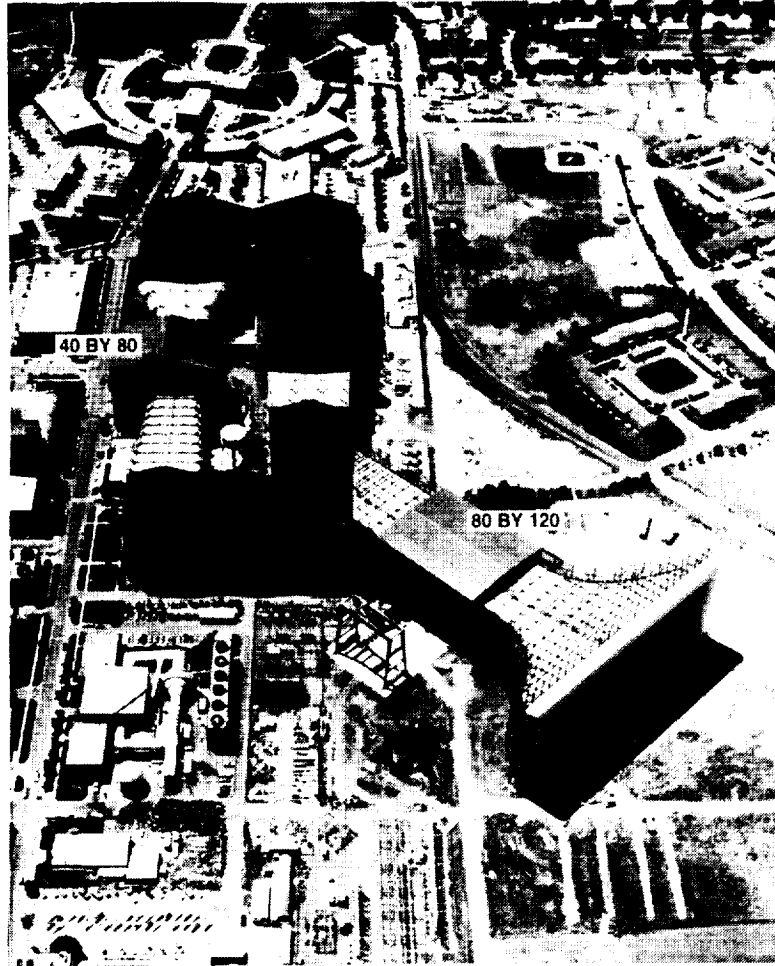
16. Soderman, P. T.; and Høglund, L. E.: Wind-Tunnel Fan Noise Reduction Including Effects of Turning Vanes on Noise Propagation. AIAA Paper 79-0642, March 1979.
17. Trebble, W. J. G.: The Acoustic Characteristics of the RAE 1.5m Wind Tunnel. RAE TR 79002, Farnborough, England, Jan. 1979.
18. Yu, J. C.; and Abrahamson, A. L.: Acoustic Treatment of the NASA Langley 4- by 7-Meter Tunnel: A Feasibility Study. NASA TP 2563, Aug. 1986.
19. Wilby, J. F. ;and White, P. H.: An Analysis of Sound Absorbing Linings for the Interior of the NASA Ames 80 x 120-Foot Wind Tunnel. NASA CR 177396, Nov. 1985.

**TABLE 1.- FAN GEOMETRY AND
OPERATION LIMITS**

	Rotor	Stator
Number of blades	15	23
Diameter	12.2 m	12.2 m
Hub-tip ratio	0.438	0.438
Root chord	1.23 m	0.89 m
Tip chord	0.90 m	0.89 m
Twist, root to tip	41.4°	5.3°
Maximum rpm	180	0
Rotor/stator spacing = 2.75 m (mid chord to mid chord)		
Fan total pressure rise, $\Delta p = 2.63 \times 10^3 \text{ N/m}^2$		

TABLE 2.- TEST SECTION ACOUSTIC LINING SPECIFICATIONS

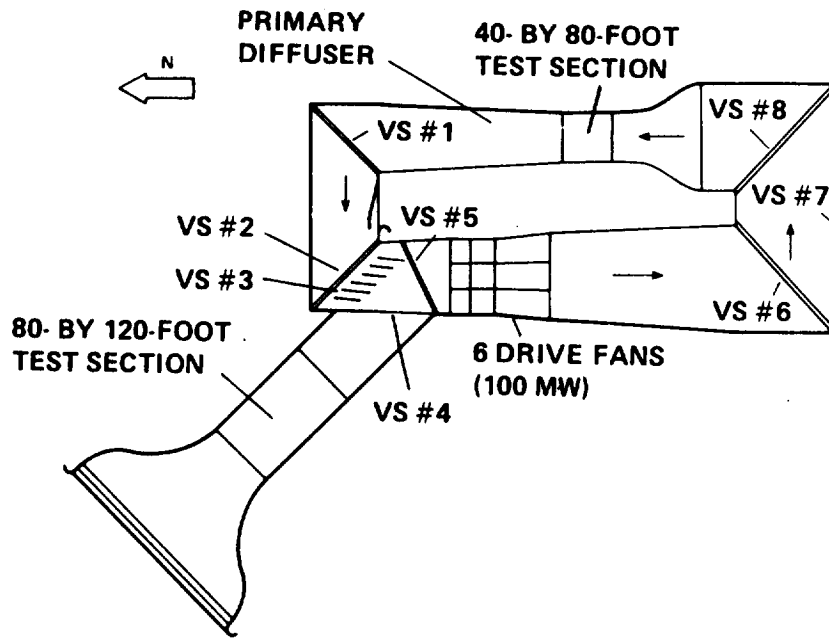
Lining depth	152 mm
Fiberglass type	Owens Corning 733
Fiberglass density	48 kg/m ³
Fiberglass flow resistivity	23,622 mks rayls/m (ref. 8) 27,000 mks rayls/m (ref. 19)
Cloth type	Uniglass 7500-50 untreated fiberglass cloth (0.32 kg/m ²)
Cloth flow resistance	13 mks rayls (estimate)
Perforated plate material (walls)	16 ga galvanized steel (1.5 mm thick)
Perforated plate material (floor)	3.18 mm thick galvanized steel
Perforated plate hole geometry	3.18 mm dia holes, 40% open area
Floor grating material	11 ga steel (3.0 mm thick)
Floor grating geometry	38 mm deep bars spaced 30.2 mm center to center in rectangular grid



a) View looking south

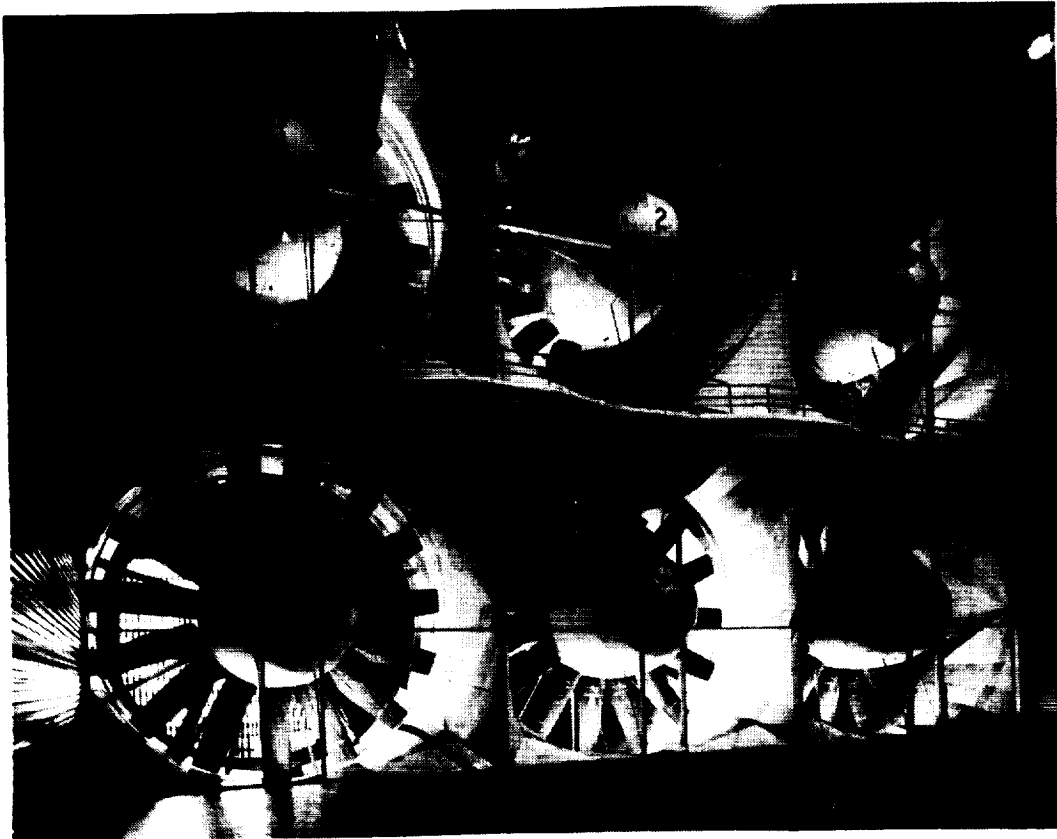
Figure 1.- 40-by 80- Foot Wind Tunnel

ORIGINAL PAGE IS
OF POOR QUALITY

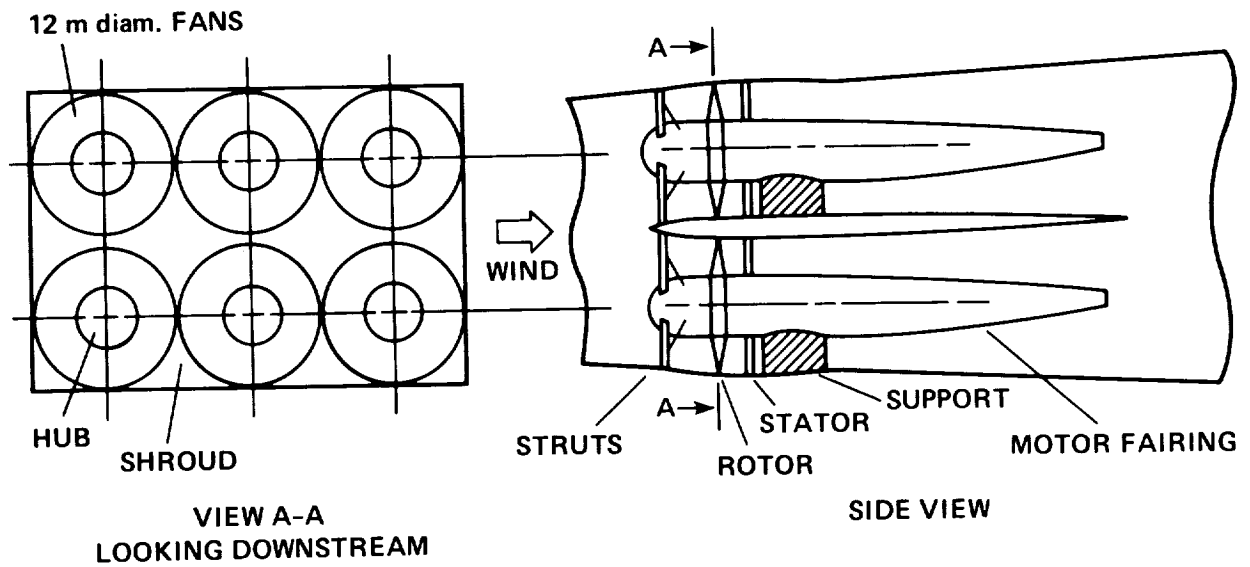


b) Circuit plan. (VS stands for vane set.)

Figure 1.- Concluded.



a) View looking downstream

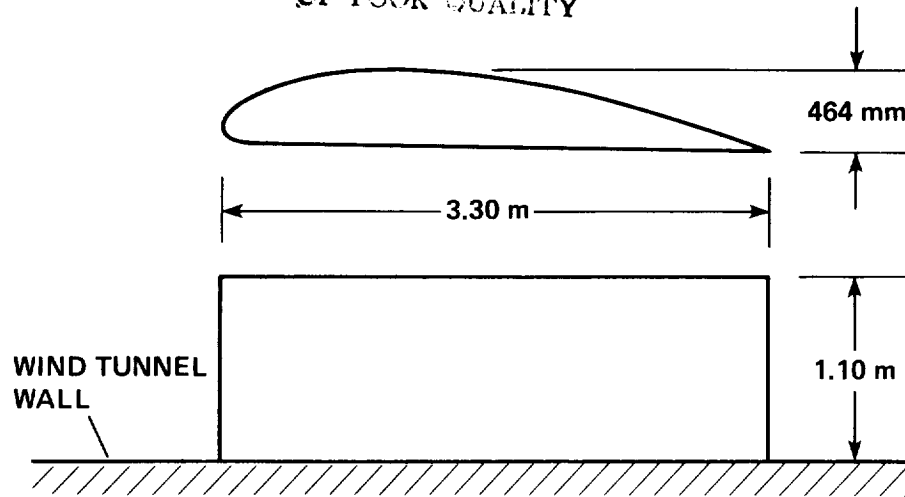


b) Schematic

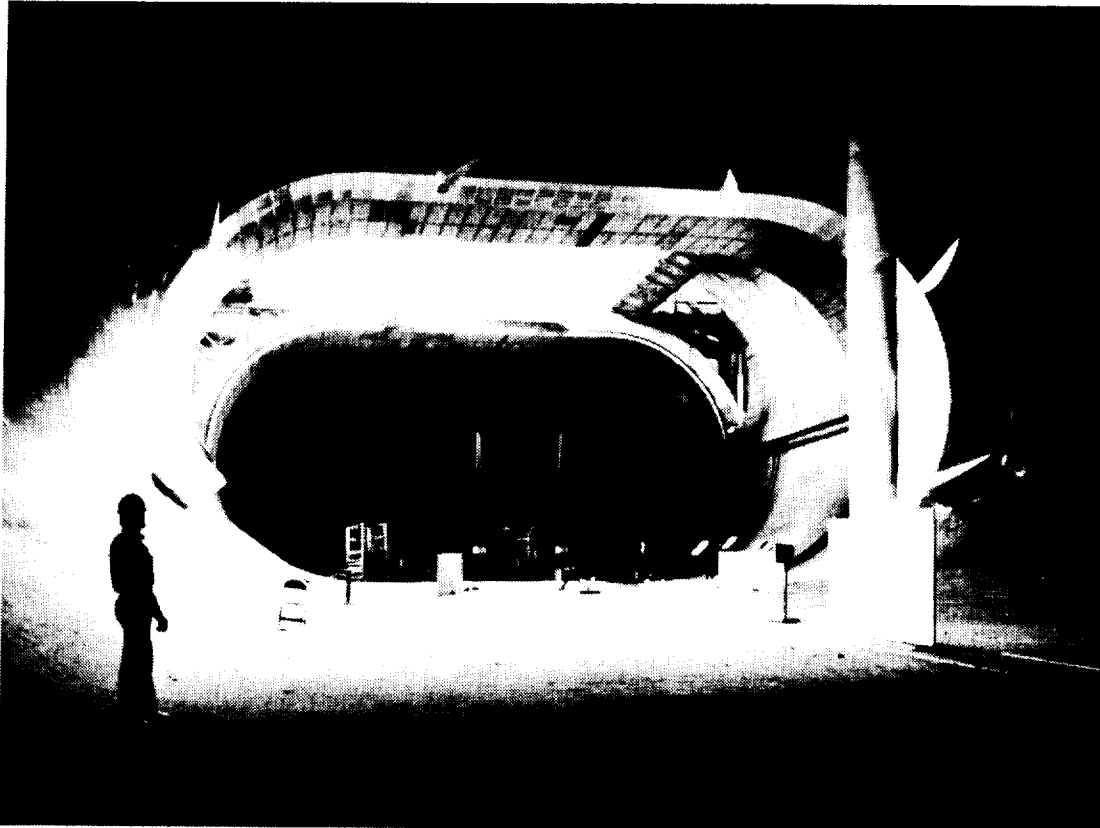
Figure 2.- Wind tunnel drive fans.

ORIGINAL PAGE IS
OF POOR QUALITY.

ORIGINAL PAGE IS
OF POOR QUALITY

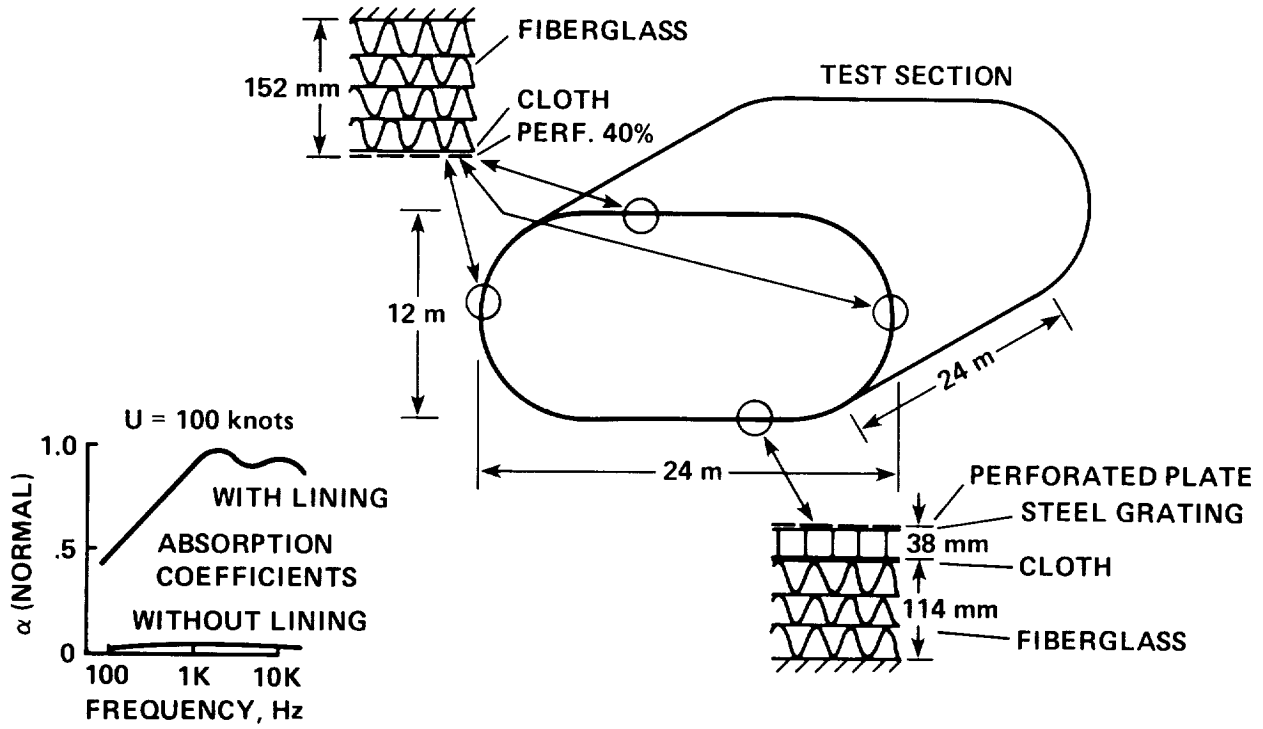


a) Shape of vortex generators



b) Vortex generators as installed at an angle of attack of 15° at a distance of 3.40 m downstream of the test section.

Figure 3.- Geometry of eight vortex generators in the primary diffuser of the 40 x 80 Foot Wind Tunnel; from ref. 7.



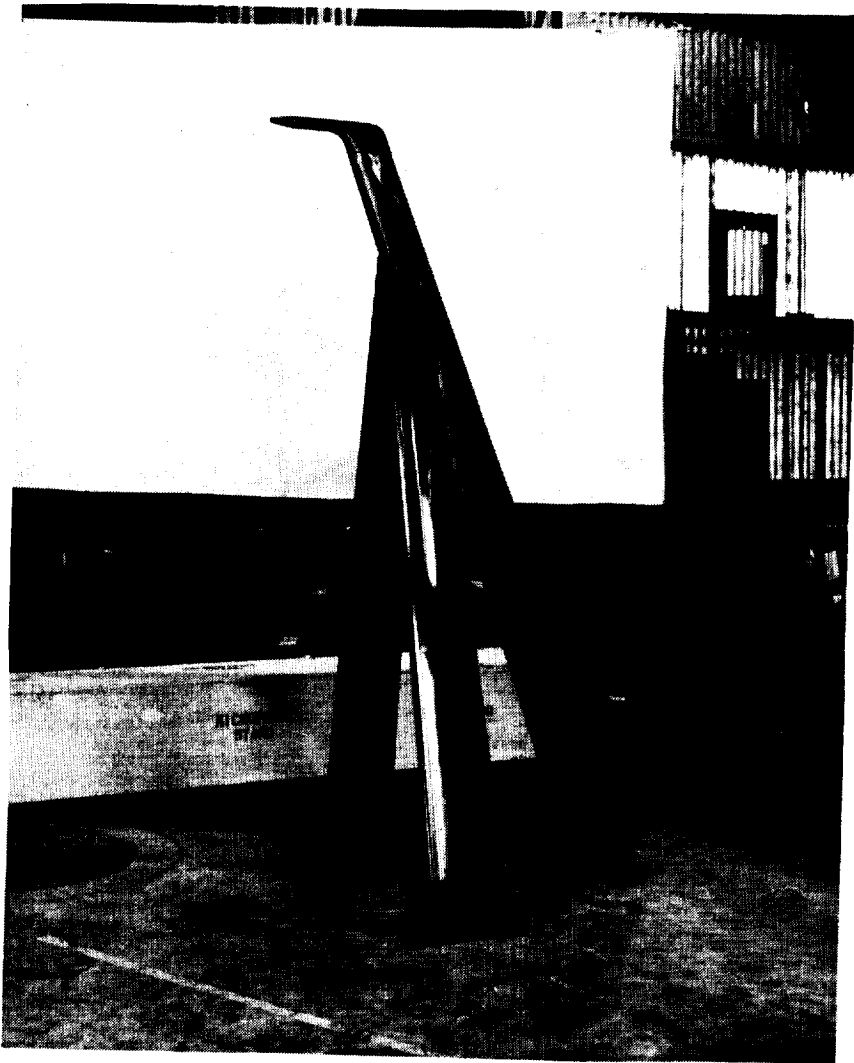
a) Lining cross section and sound absorption



b) View looking downstream in test section. Flow survey rig installed.

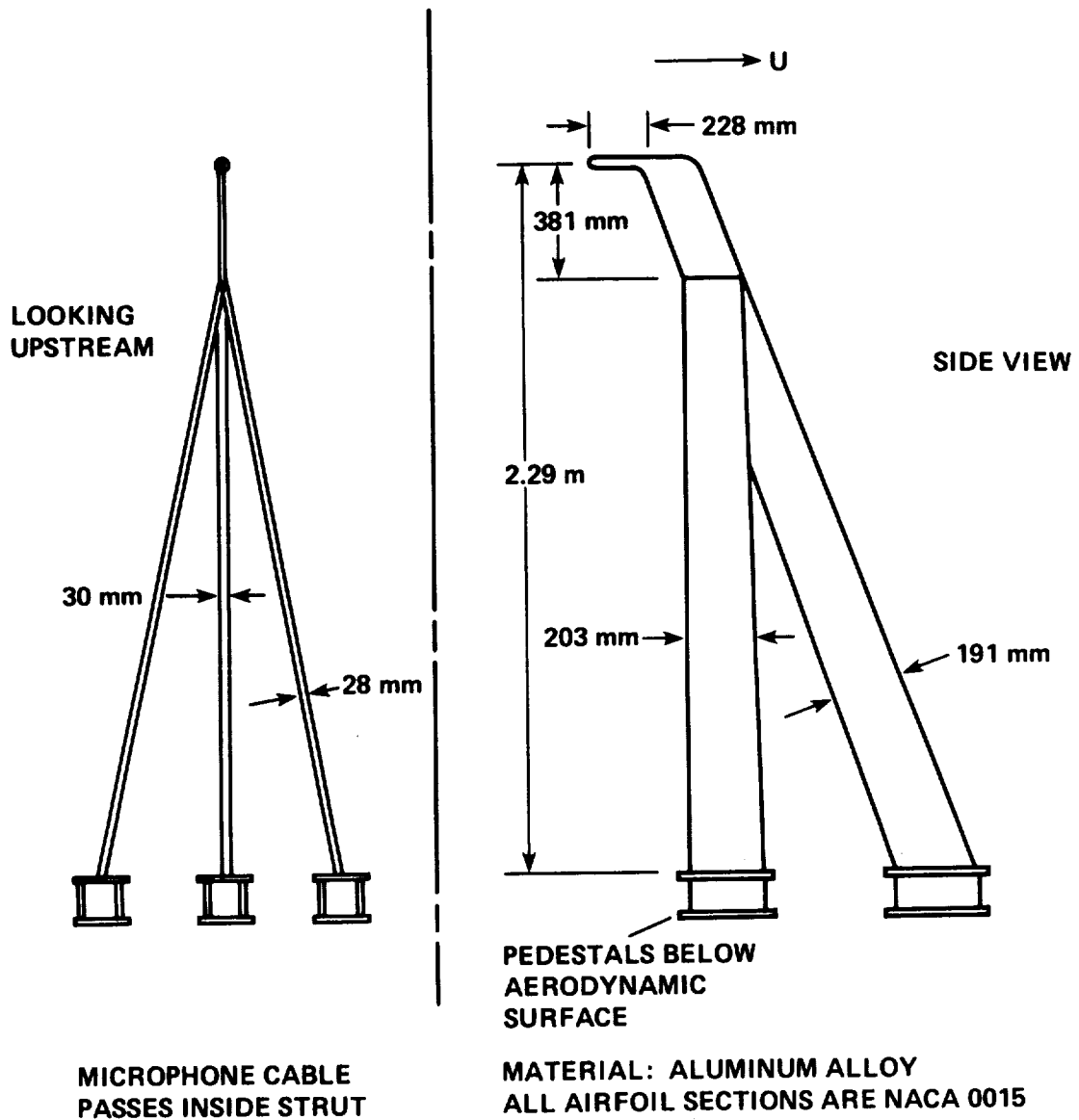
Figure 4.- Test-section acoustic lining.

ORIGINAL PAGE IS
OF POOR QUALITY



a) Photo

Figure 5.- Microphone strut.



b) Schematic

Figure 5.- Concluded.

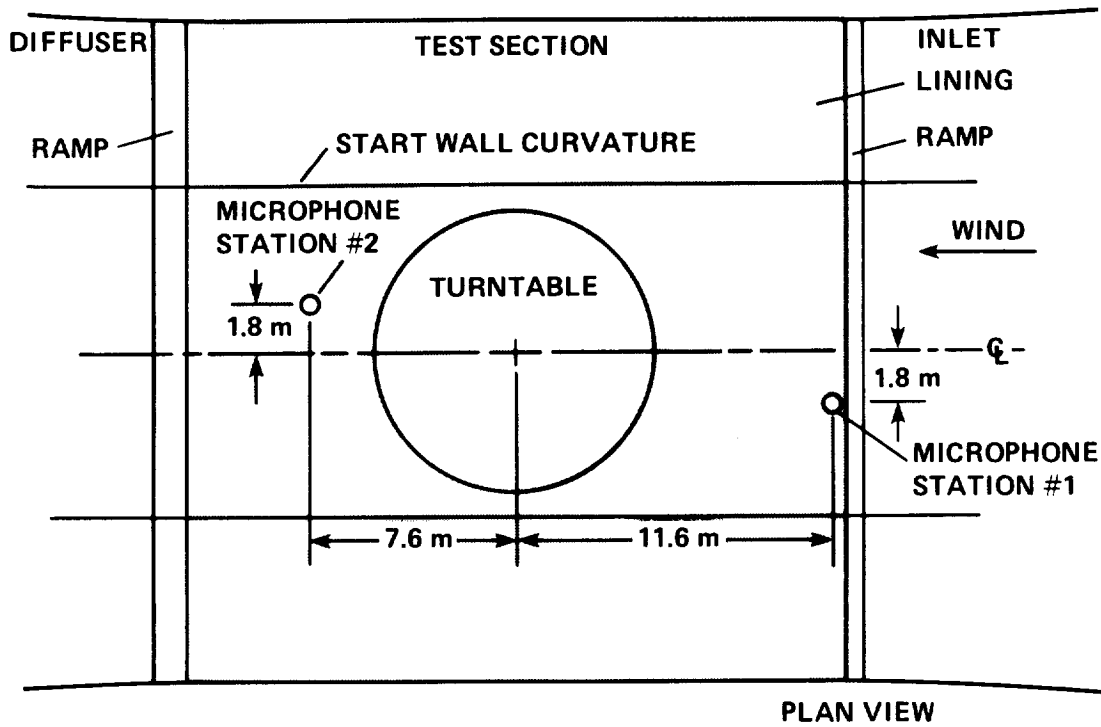


Figure 6.- Microphone locations in the test section. The microphone was moved from station #1 to station #2.

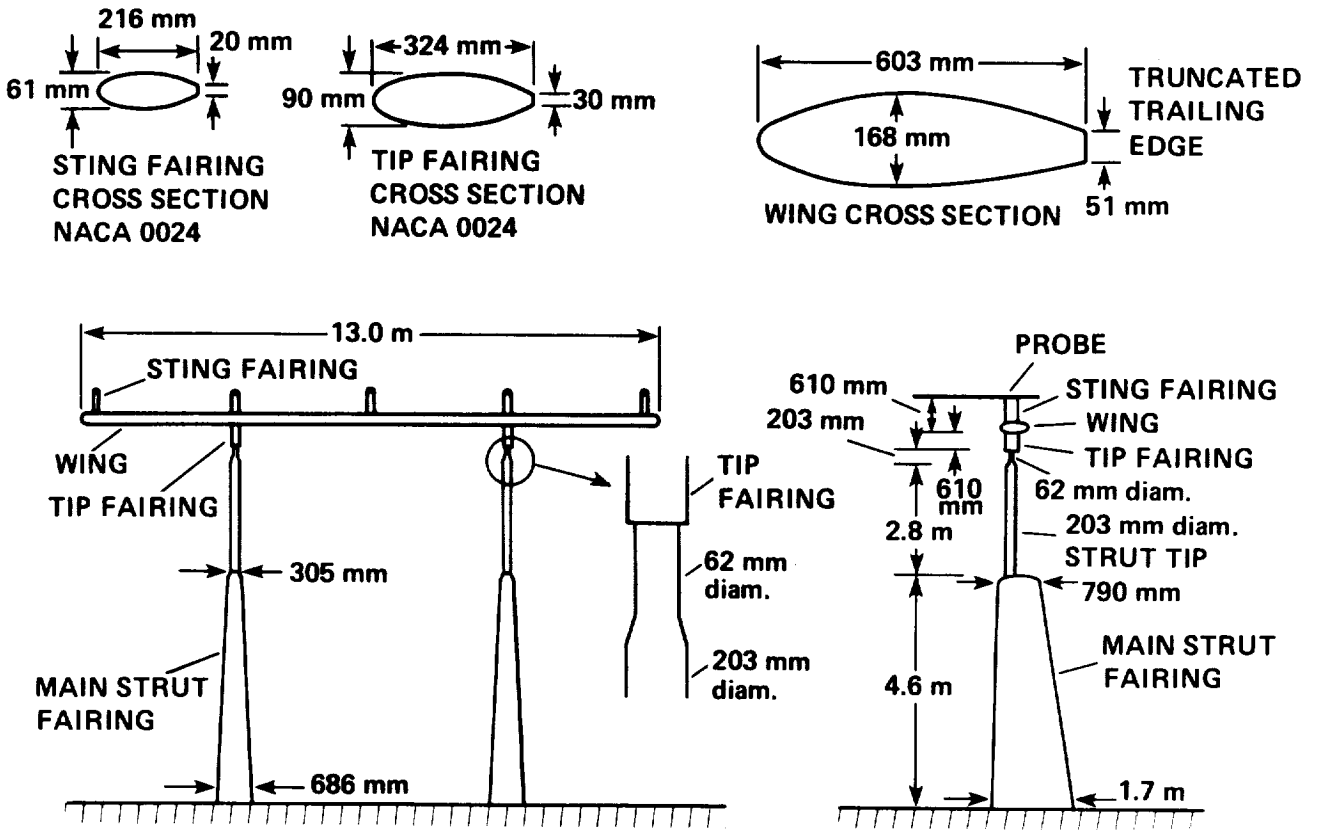


Figure 7.- Wind tunnel flow survey rig.

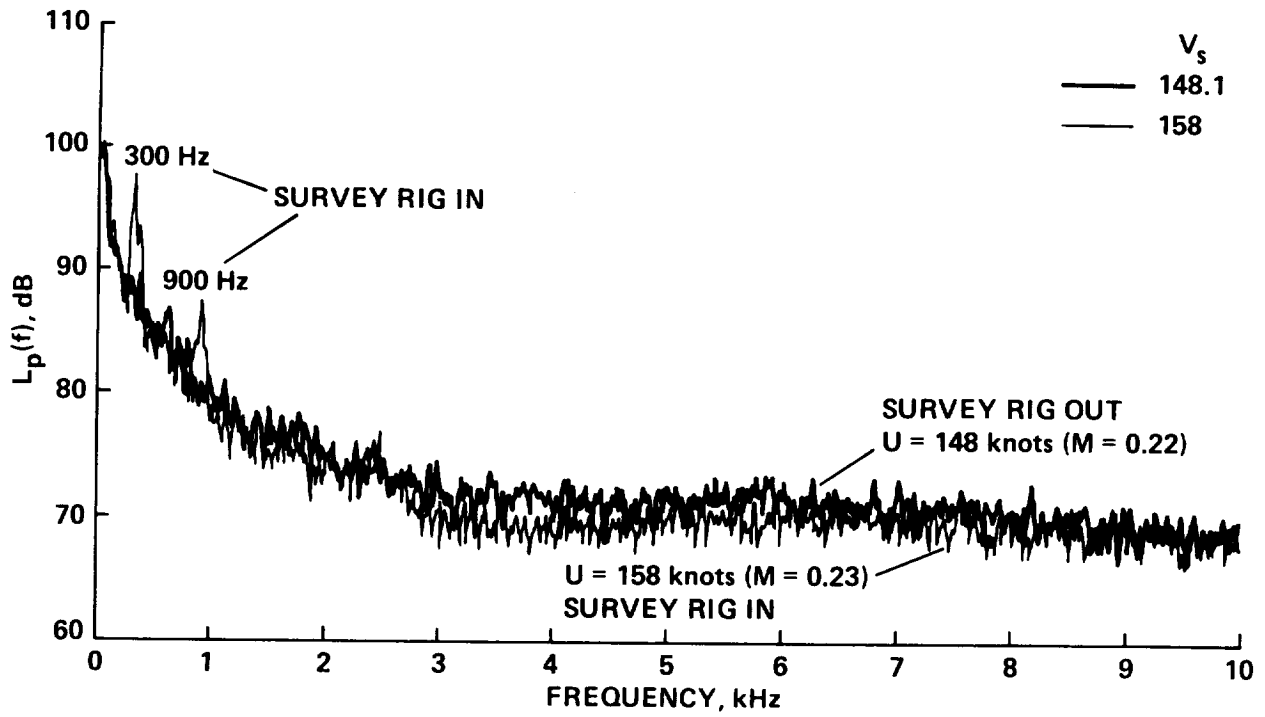


Figure 8.- Test-section noise spectrum with and without survey rig installed; microphone at station #1.
 $N = 180, \beta = 24^\circ$.

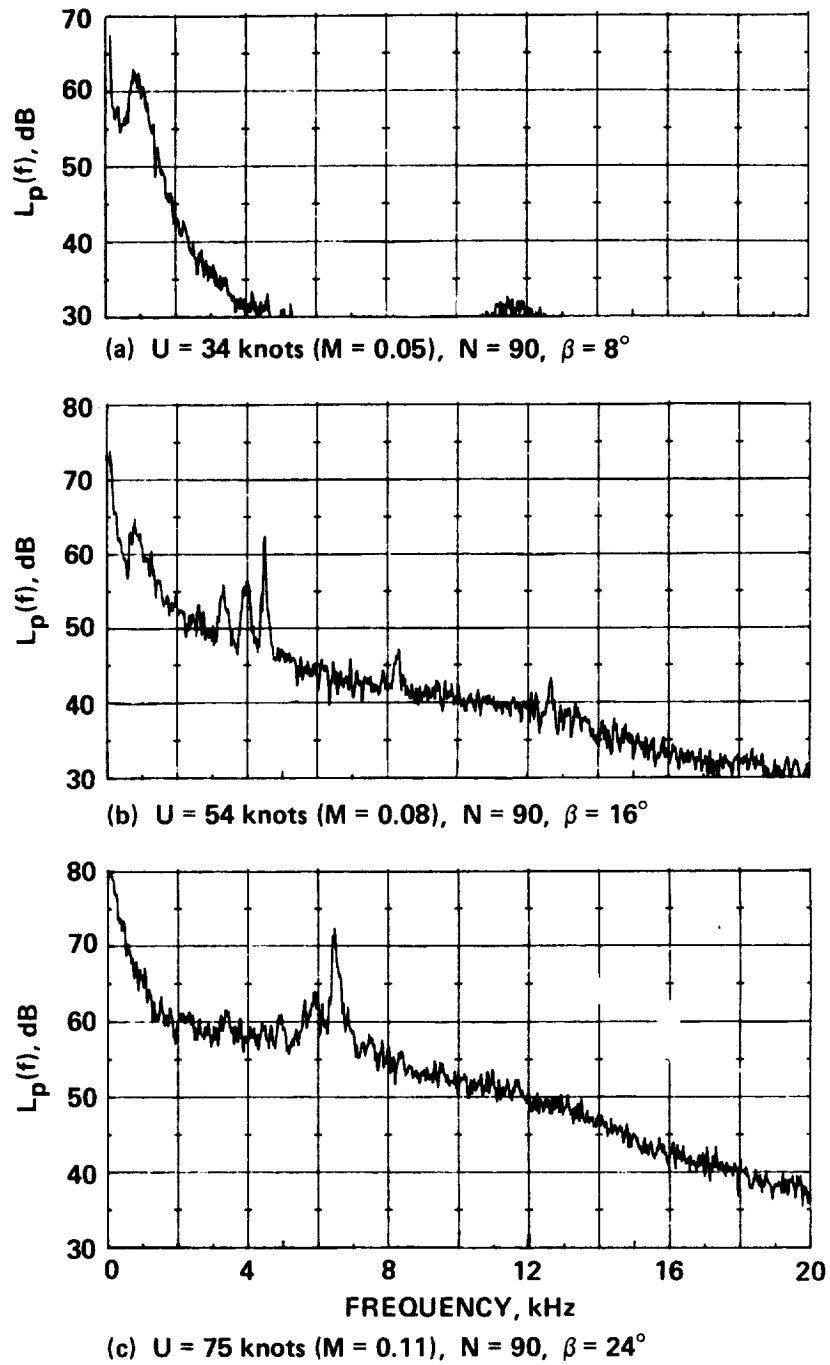
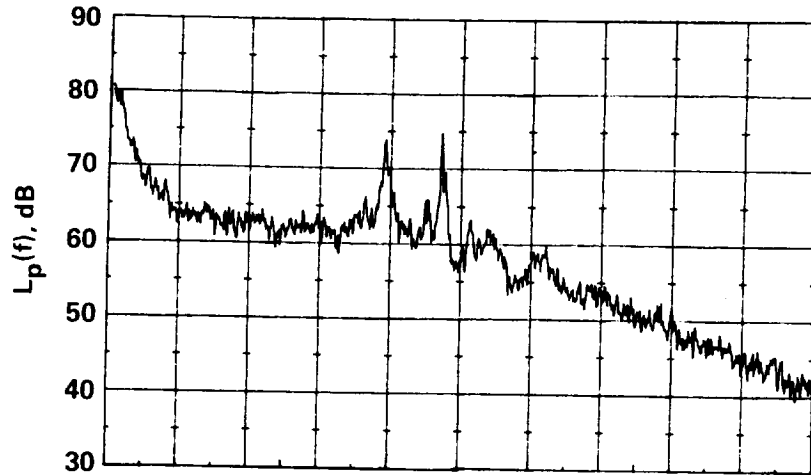
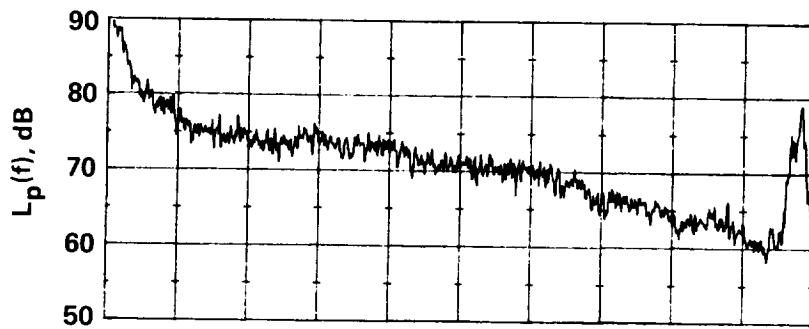


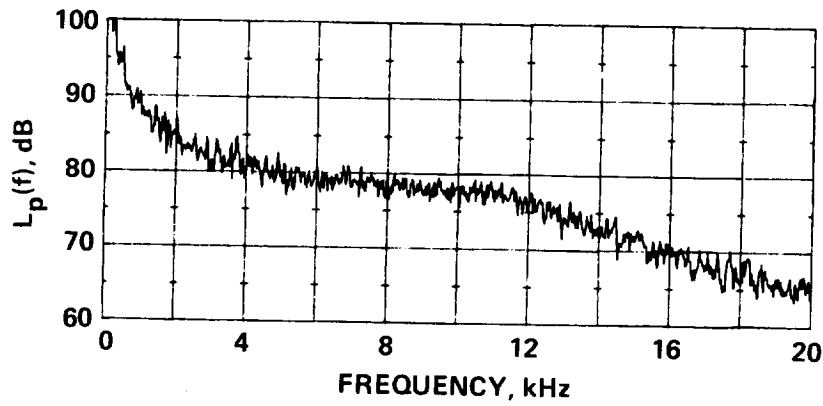
Figure 9.- Empty test-section noise spectra 10 - 20 kHz measured at station #1 for several airspeeds.



(d) $U = 91$ knots ($M = 0.14$), $N = 90$, $\beta = 30^\circ$

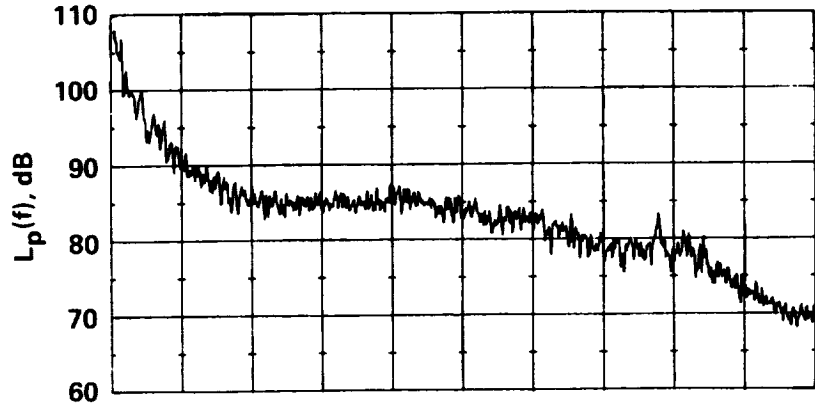


(e) $U = 148$ knots ($M = 0.22$), $N = 180$, $\beta = 24^\circ$

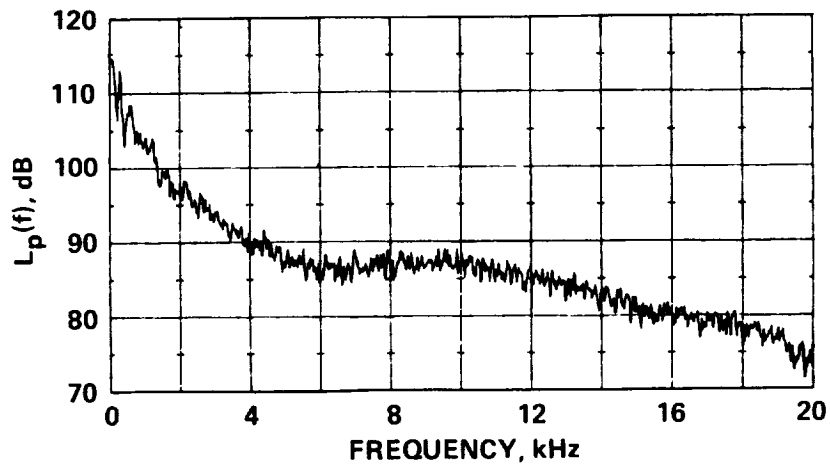


(f) $U = 191$ knots ($M = 0.29$), $N = 180$, $\beta = 32^\circ$

Figure 9.- Continued.

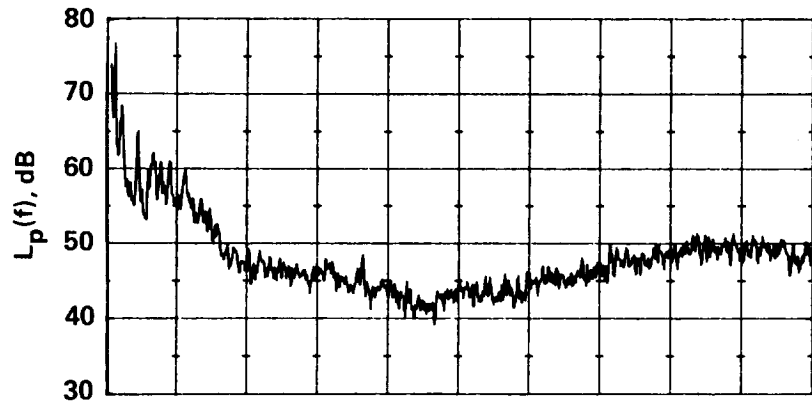


(g) $U = 234$ knots ($M = 0.35$), $N = 180$, $\beta = 40^\circ$

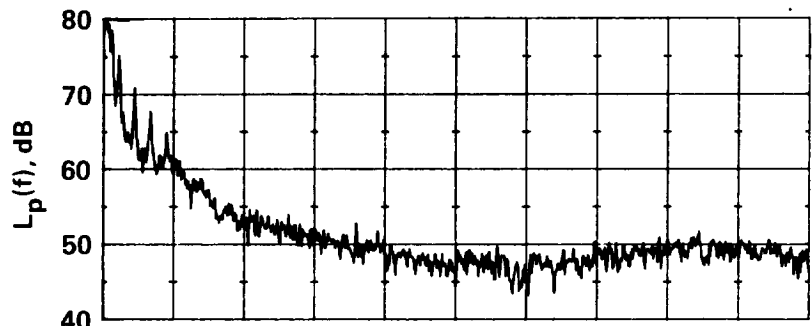


(h) $U = 274$ knots ($M = 0.40$), $N = 180$, $\beta = 48^\circ$

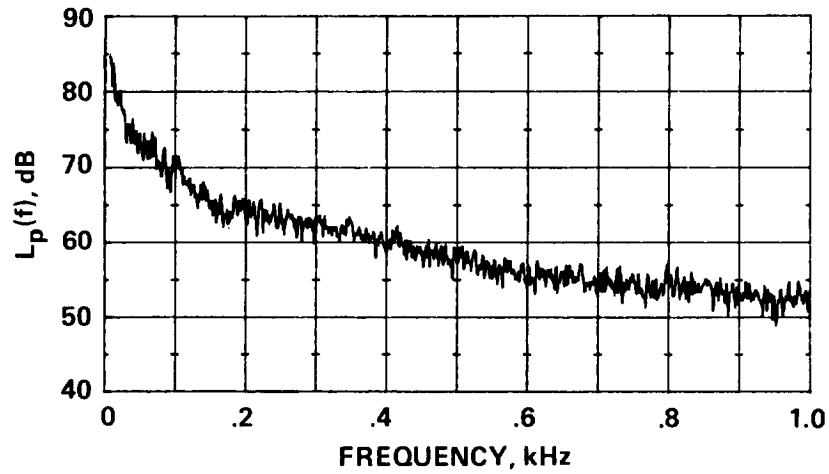
Figure 9.- Concluded.



(a) $U = 34$ knots ($M = 0.05$), $N = 90$, $\beta = 8^\circ$

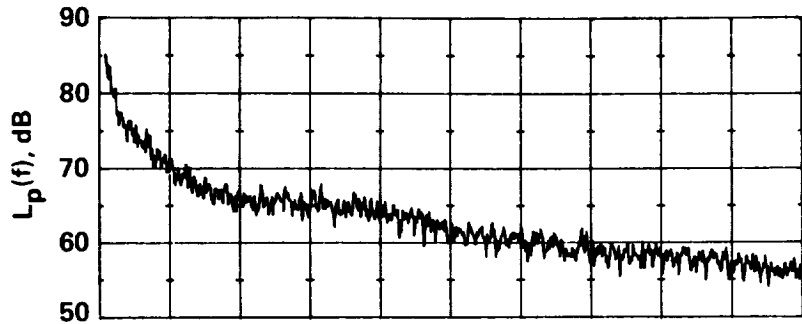


(b) $U = 54$ knots ($M = 0.08$), $N = 90$, $\beta = 16^\circ$

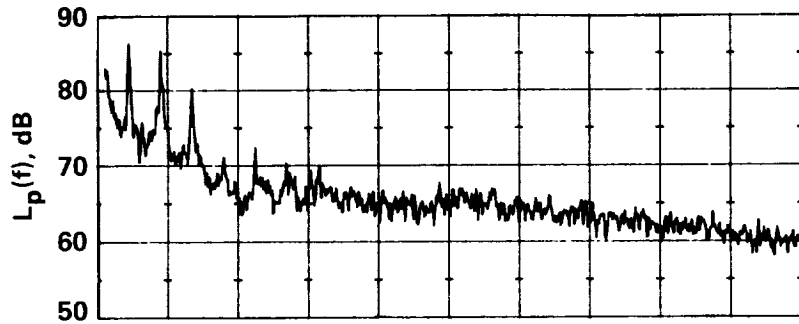


(c) $U = 75$ knots ($M = 0.11$), $N = 90$, $\beta = 24^\circ$

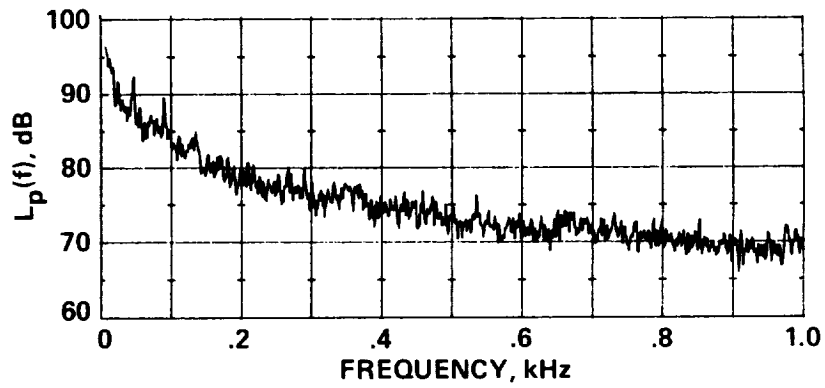
Figure 10.- Empty test-section noise spectra 10 - 1 kHz measured at station #1 for several airspeeds.



(d) $U = 91$ knots ($M = 0.14$), $N = 90$, $\beta = 30^\circ$

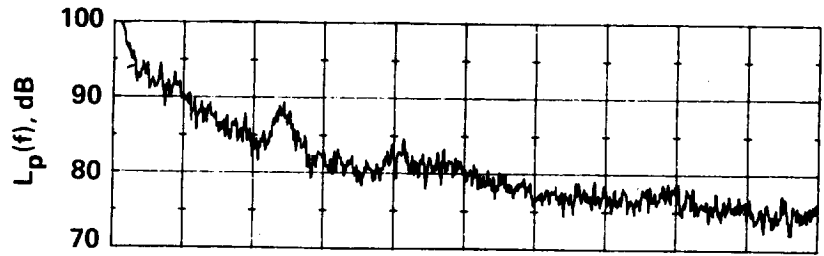


(e) $U = 75$ knots ($M = 0.11$), $N = 180$, $\beta = 10^\circ$

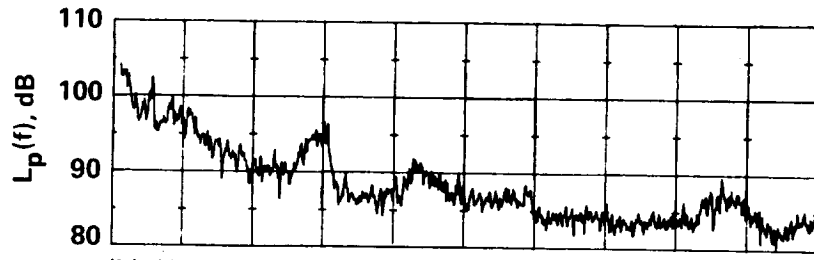


(f) $U = 148$ knots ($M = 0.22$), $N = 180$, $\beta = 24^\circ$

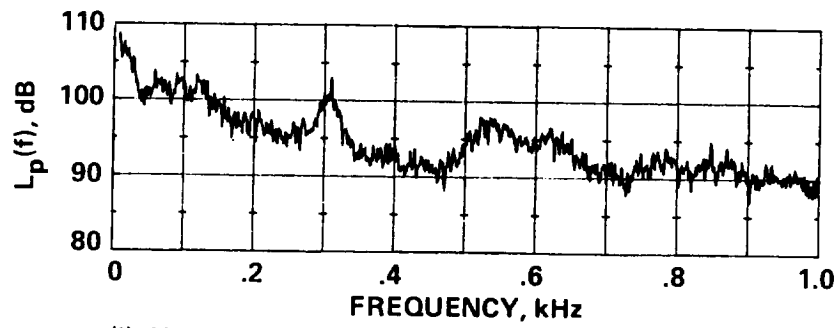
Figure 10.- Continued.



(g) $U = 191$ knots ($M = 0.29$), $N = 180$, $\beta = 32^\circ$



(h) $U = 234$ knots ($M = 0.35$), $N = 180$, $\beta = 40^\circ$



(i) $U = 274$ knots ($M = 0.40$), $N = 180$, $\beta = 48^\circ$

Figure 10.- Concluded.

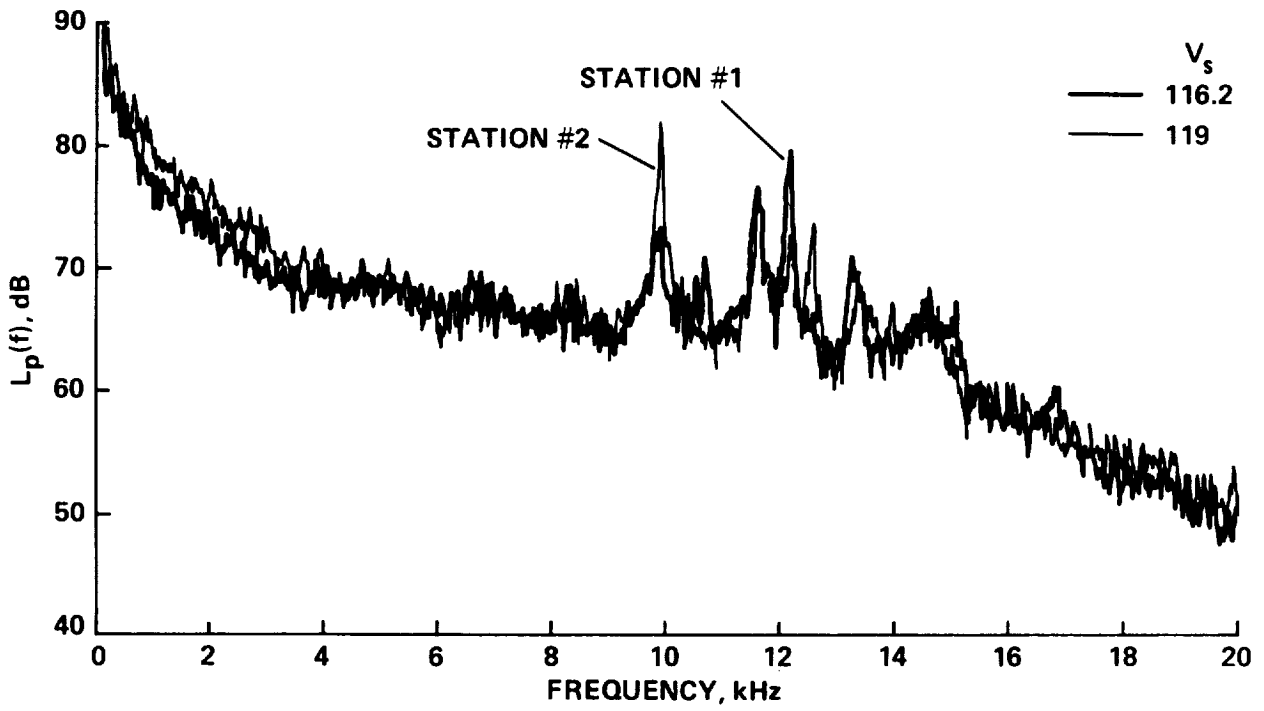


Figure 11.- A comparison of acoustic spectra measured upstream (station #1) and downstream (station #2) in the empty test section; $U = 117$ knots ($M = 0.18$), $N = 180$, $\beta = 18^\circ$.

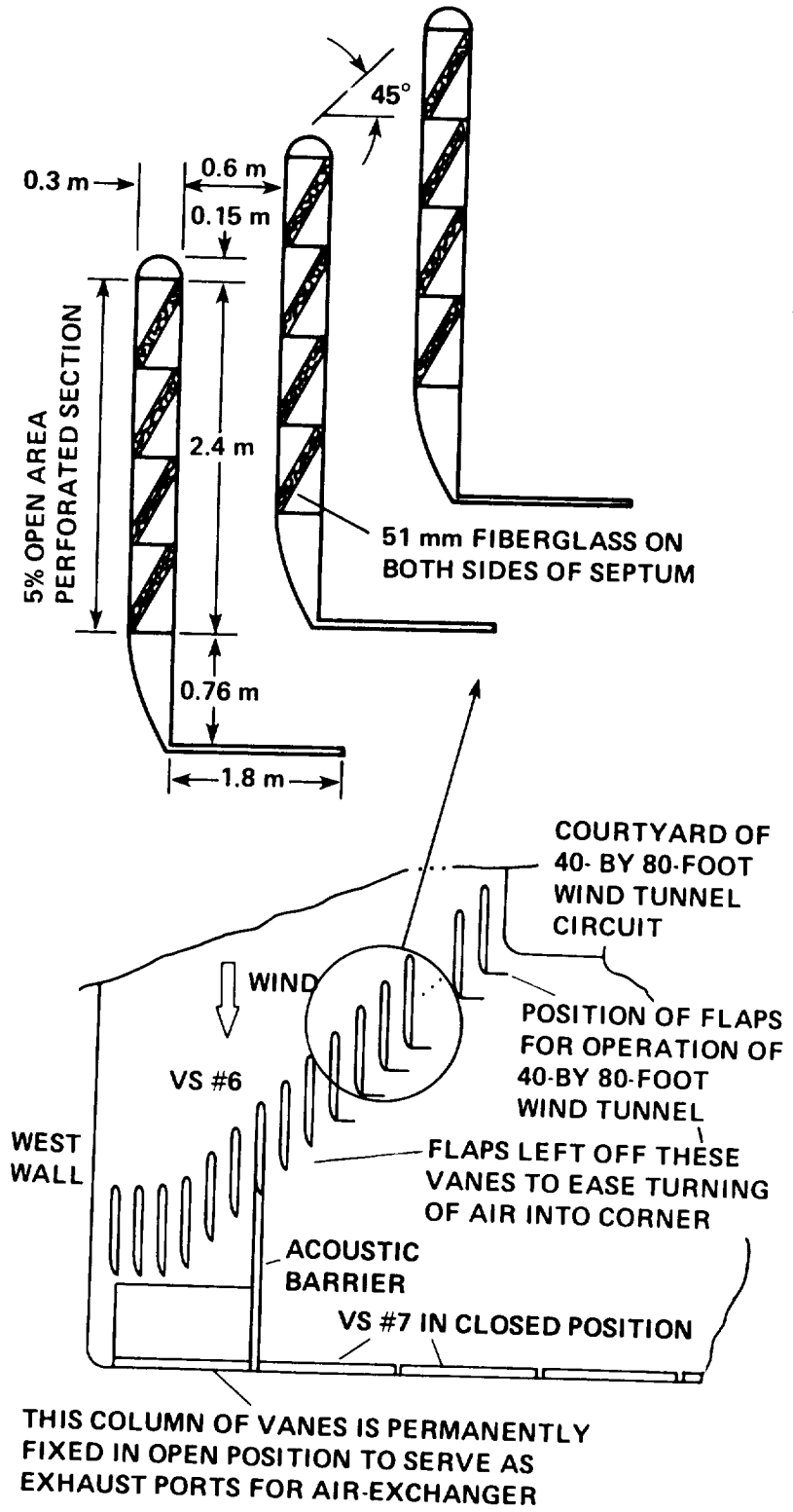


Figure 12.- Acoustically treated vanes which comprise vane set 6 (first vane set downstream of the drive fans).

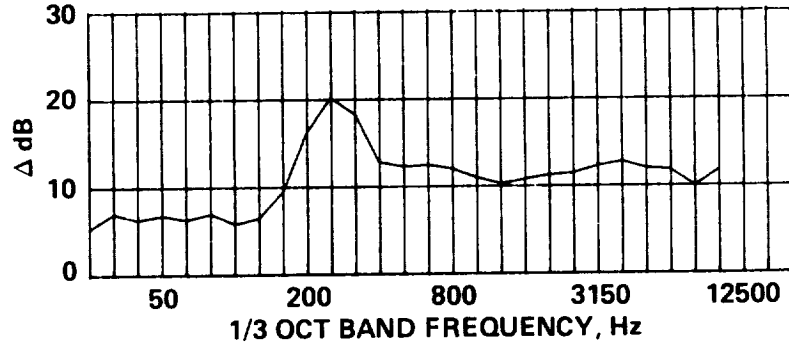


Figure 13.- Noise reduction of the acoustically treated vane set 6 as measured in the west and south legs of the circuit; $N = 175$, $\beta = 0^\circ$.

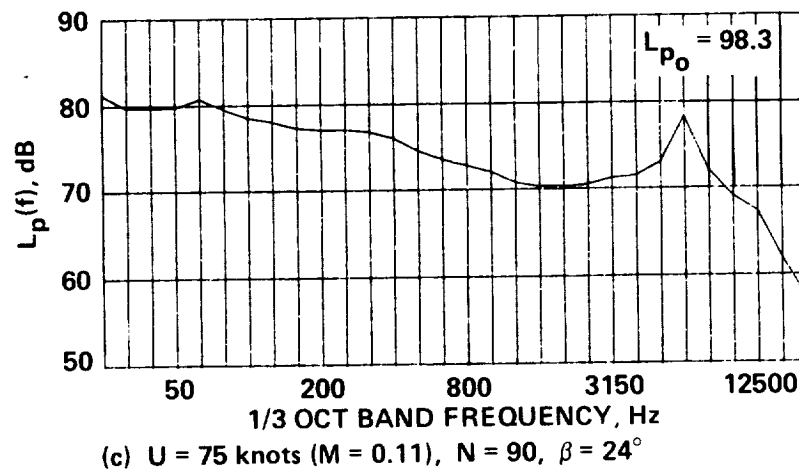
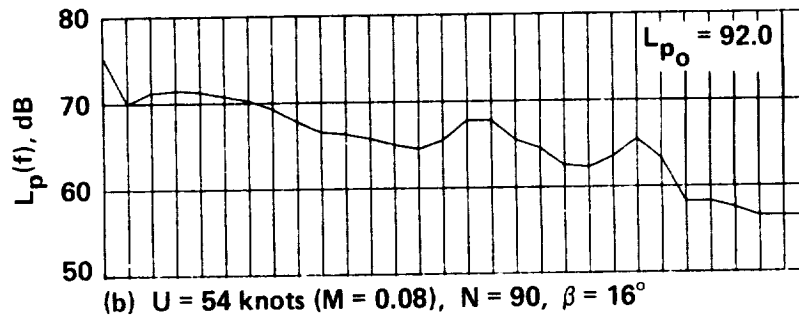
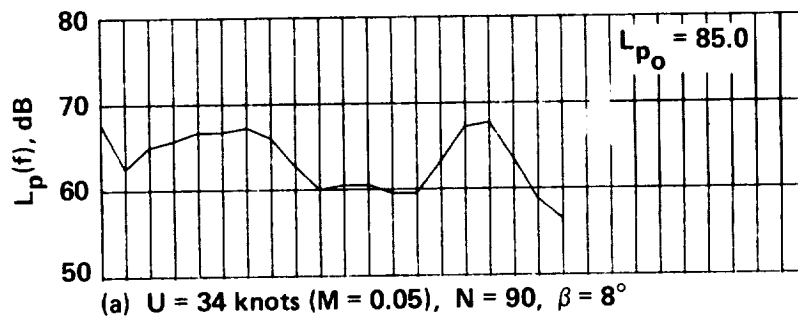
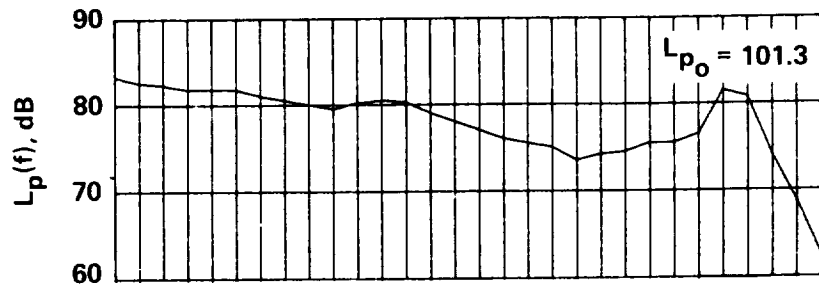
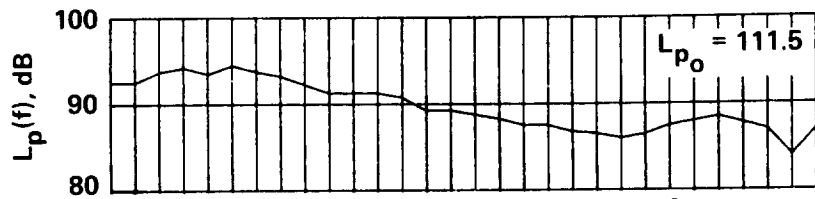


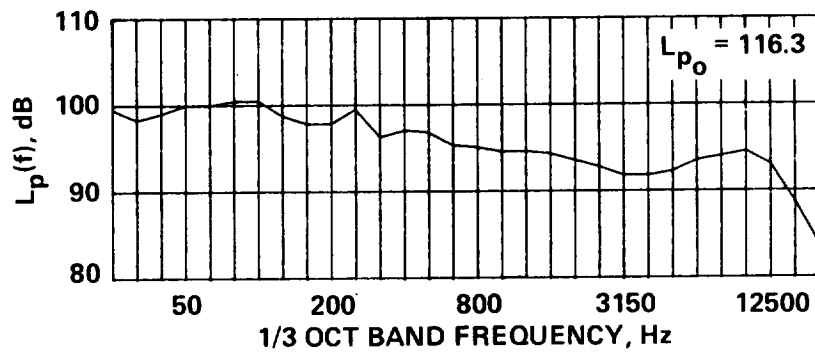
Figure 14.- Empty test-section third-octave band noise spectra measured at station #1 for several airspeeds (equivalent to narrow band spectra in figures 9 (a)-(h)).



(d) $U = 91$ knots ($M = 0.14$), $N = 90$, $\beta = 30^\circ$

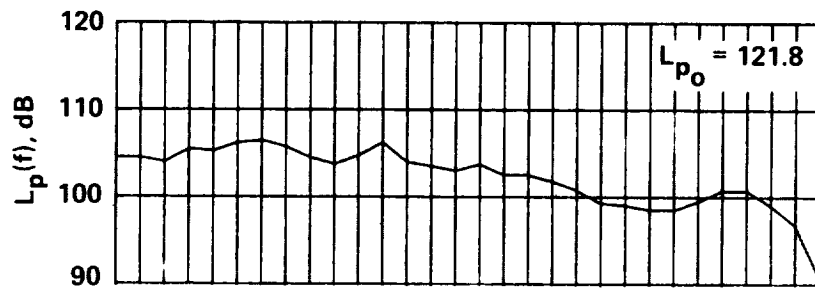


(e) $U = 148$ knots ($M = 0.22$), $N = 180$, $\beta = 24^\circ$

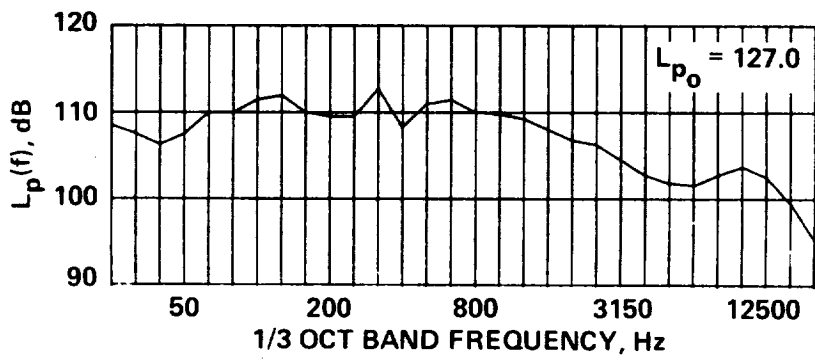


(f) $U = 191$ knots ($M = 0.29$), $N = 180$, $\beta = 32^\circ$

Figure 14.- Continued.



(g) $U = 234$ knots ($M = 0.35$), $N = 180$, $\beta = 40^\circ$



(h) $U = 274$ knots ($M = 0.40$), $N = 180$, $\beta = 48^\circ$

Figure 14.- Concluded.

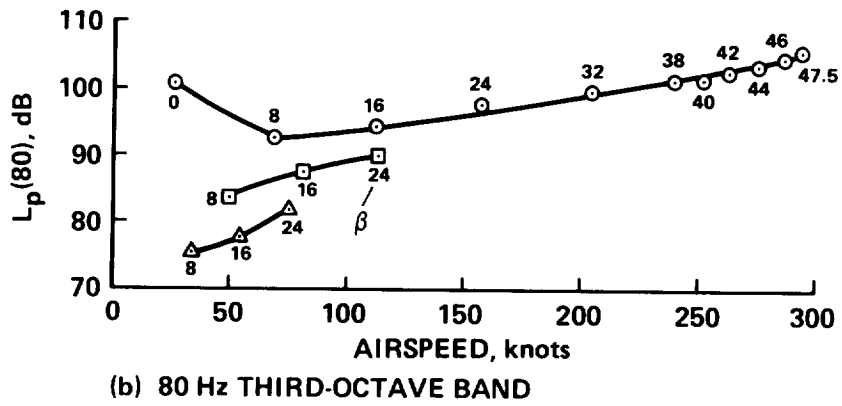
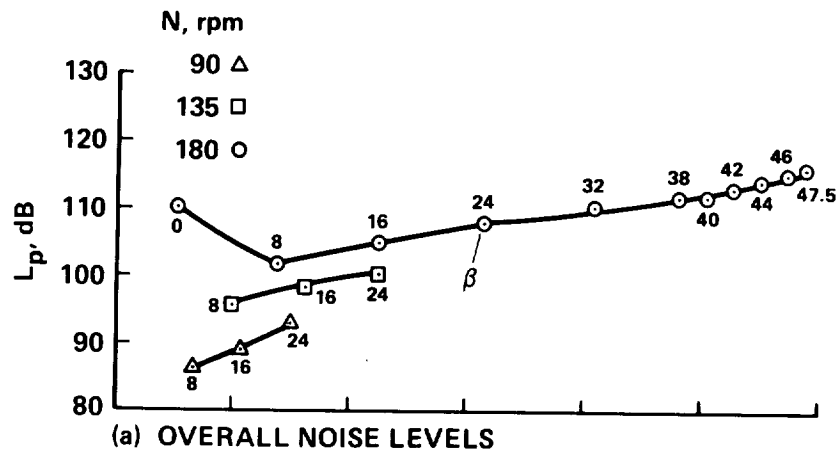


Figure 15.- Noise in the west leg downstream of fan drive versus test-section airspeed. Fan blade pitch was varied; fan speed was held at 90, 135, or 180 rpm

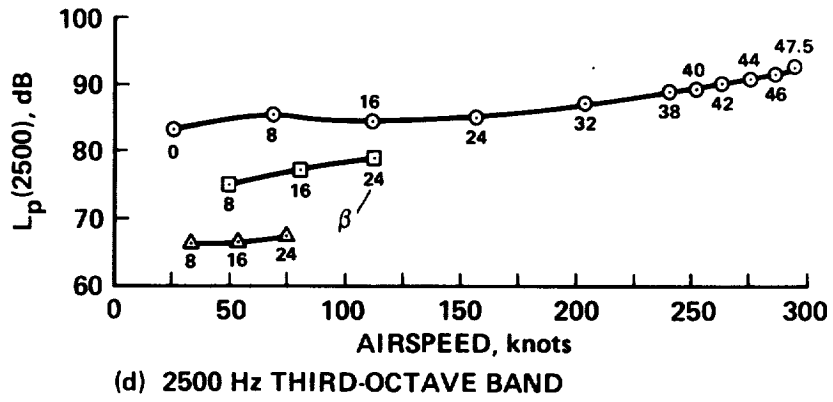
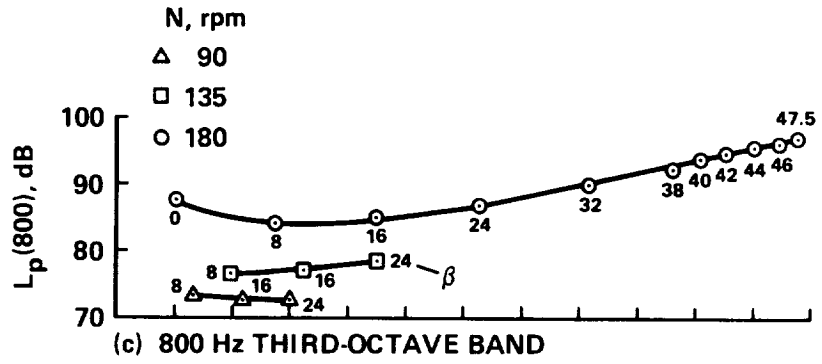
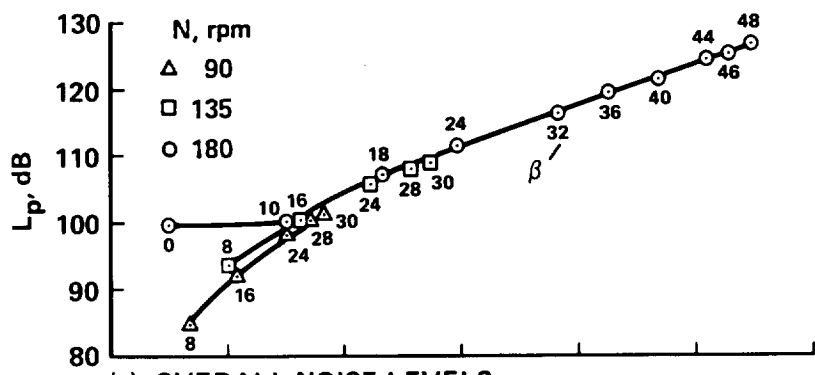
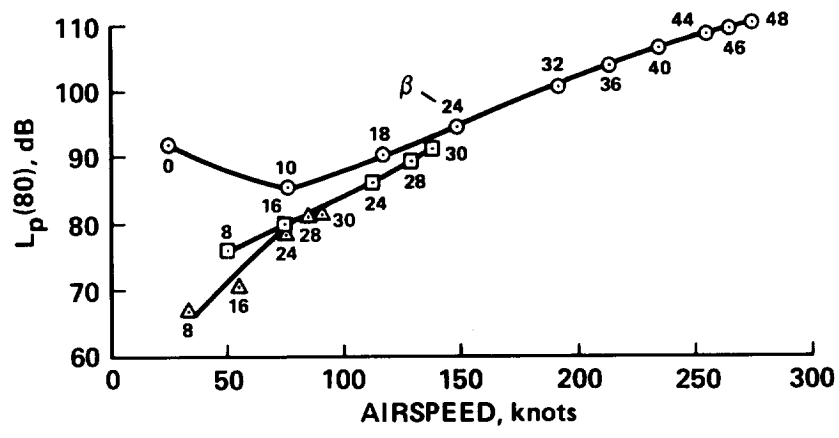


Figure 15.- Concluded.

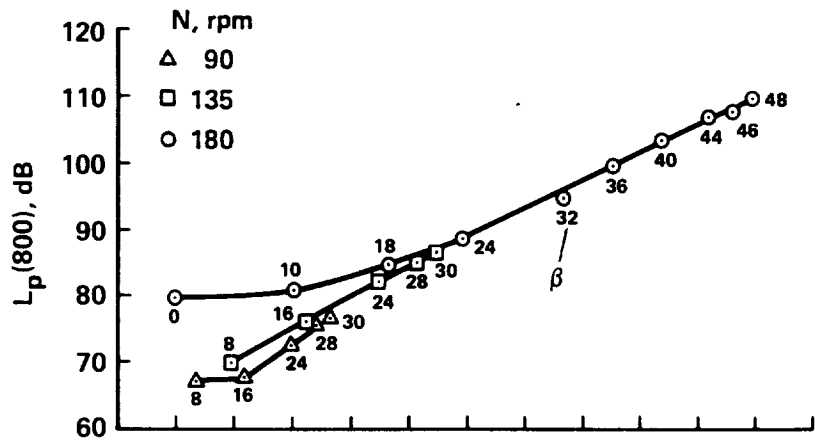


(a) OVERALL NOISE LEVELS

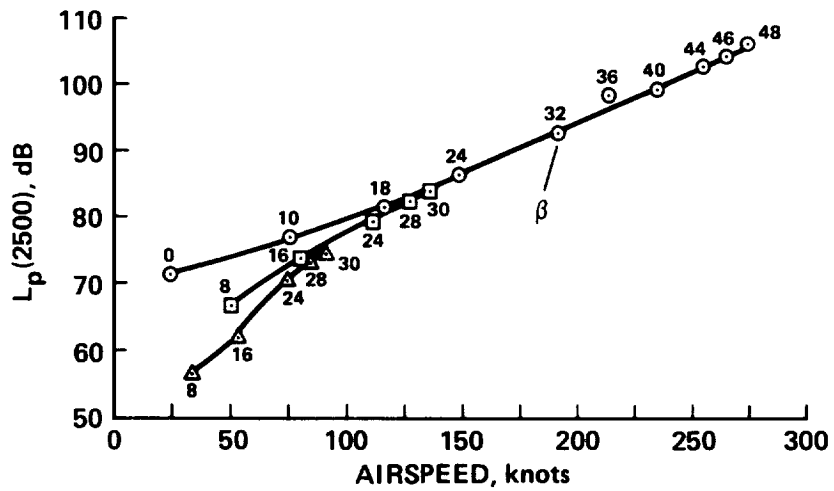


(b) 80 Hz THIRD-OCTAVE BAND

Figure 16.- Test-section noise variation with airspeed; microphone at station #1 in the empty test section. Fan blade pitch was varied; fan speed was held at 90, 135, or 180 rpm



(c) 800 Hz THIRD-OCTAVE BAND



(d) 2500 Hz THIRD-OCTAVE BAND

Figure 16.- Concluded.

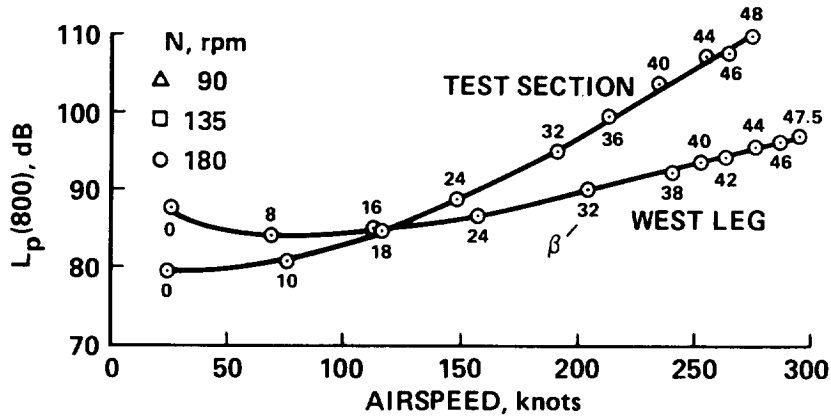


Figure 17.- A comparison of west-leg and test-section noise variation with test-section airspeed at 180 rpm fan speed; 800 Hz third-octave band.

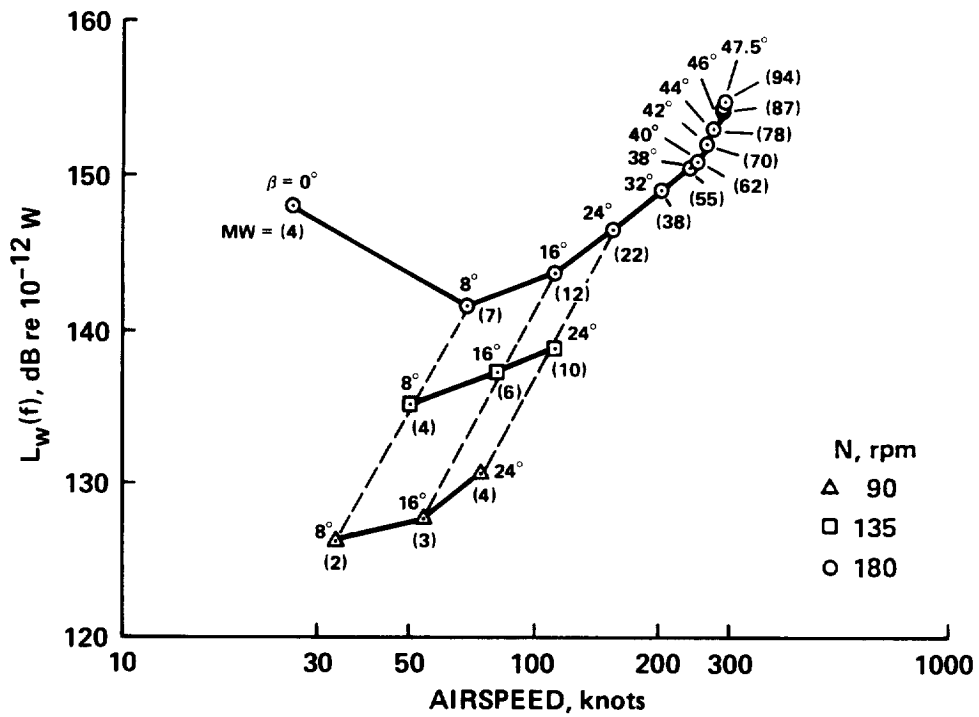


Figure 18.- Fan sound power variation with test-section airspeed. Blade pitch angle (β) and fan drive electrical consumption (MW) are noted. The solid lines correspond to fan operation at constant rotational speed, the dashed lines correspond to operation at constant pitch.

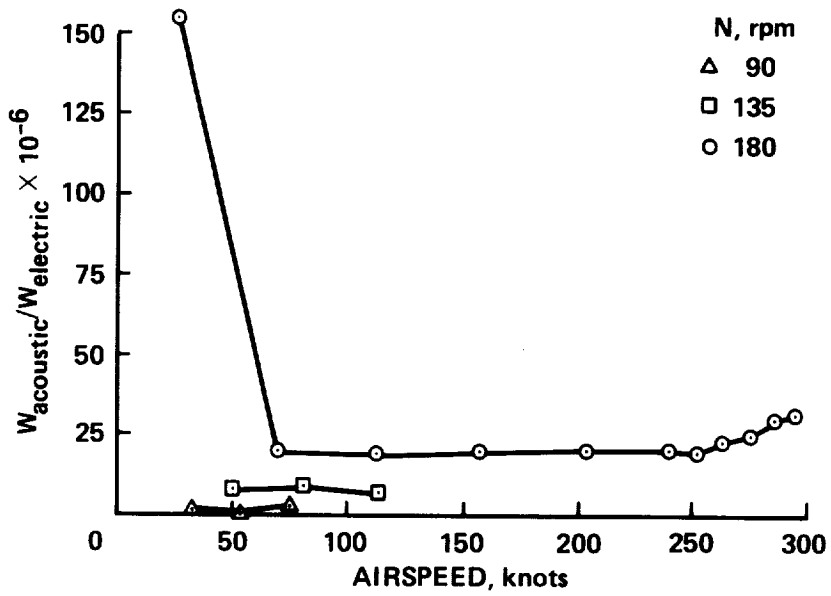


Figure 19.- Fan acoustic efficiency (acoustic power/electrical power consumption, both in Watts).

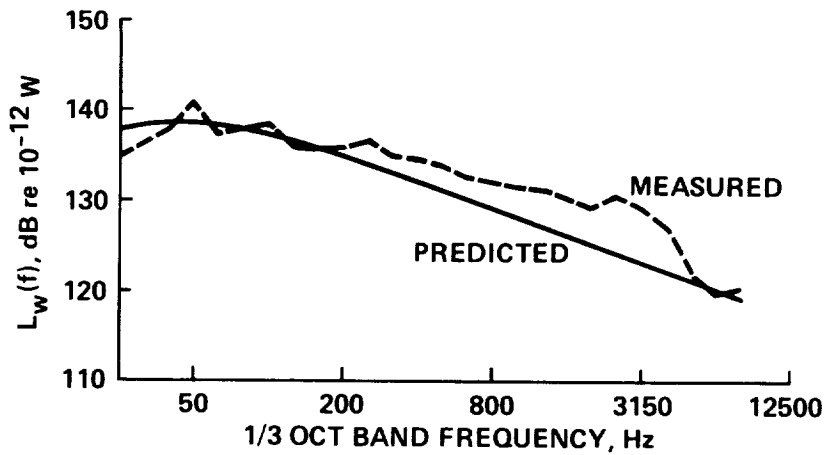


Figure 20.- Fan-drive third-octave sound power spectrum as measured and predicted using empirical equation (6); $N = 180$, $\beta = 32^\circ$.

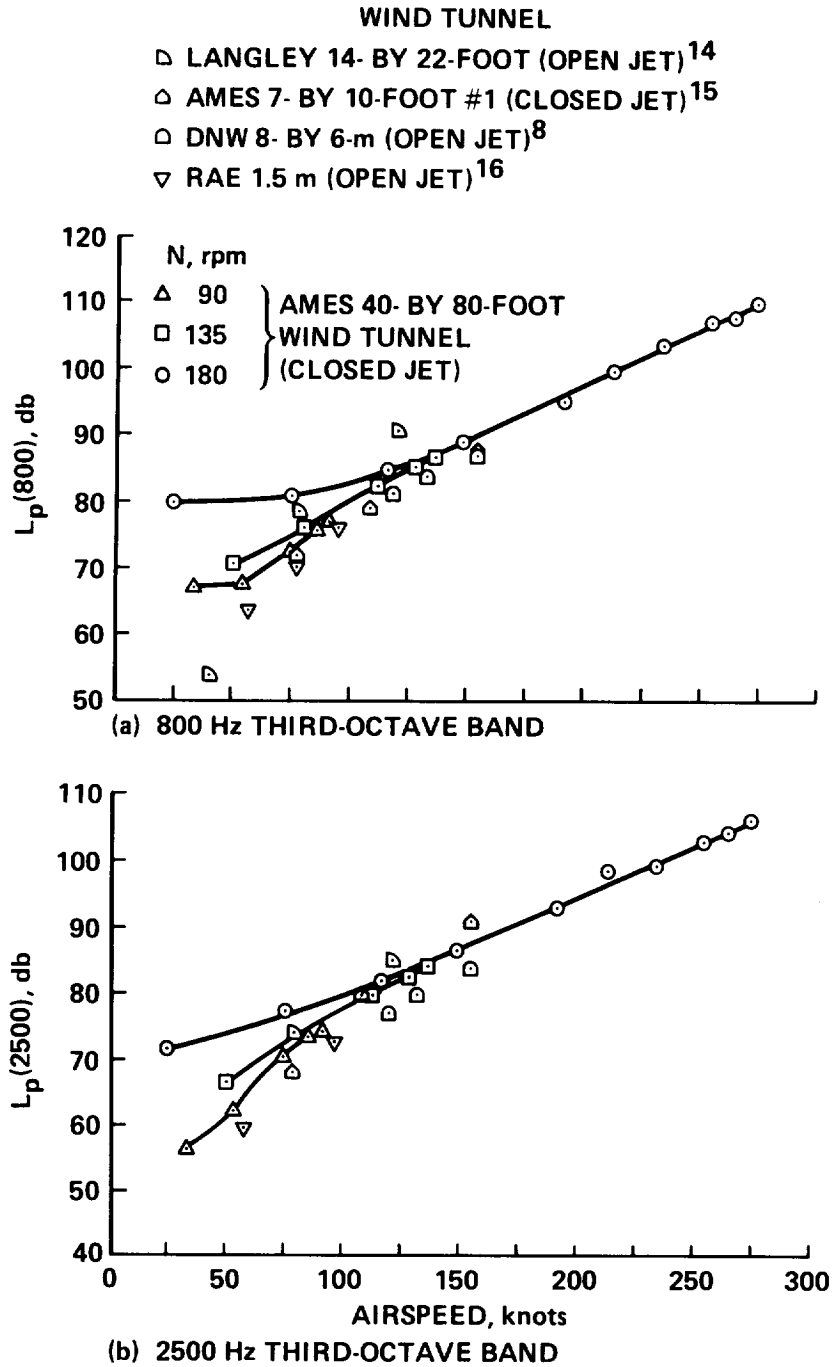


Figure 21.- A comparison of in-flow background noise versus airspeed from five wind tunnels.



Report Documentation Page

1. Report No. NASA TM-100077	2. Government Accession No.	3. Recipient's Catalog No.	
4. Title and Subtitle Sources and Levels of Background Noise in the NASA Ames 40- by 80-Foot Wind Tunnel - A Status Report		5. Report Date May 1988	
		6. Performing Organization Code	
7. Author(s) Paul T. Soderman		8. Performing Organization Report No. A-88112	
		10. Work Unit No. 505-61-11	
9. Performing Organization Name and Address Ames Research Center Moffett Field, CA 94035		11. Contract or Grant No.	
		13. Type of Report and Period Covered Technical Memorandum	
12. Sponsoring Agency Name and Address National Aeronautics and Space Administration Washington, DC 20546-0001		14. Sponsoring Agency Code	
		15. Supplementary Notes Point of Contact: Paul T. Soderman, Ames Research Center, MS 247-2 Moffett Field, CA 94035 (415) 694-6675 or FTS 464-6675	
16. Abstract <p>Background noise levels have been measured in the NASA Ames Research Center 40- by 80-Foot Wind Tunnel following installation of a sound-absorbent lining on the test-section walls. Results show that the fan-drive noise dominated the empty test-section background noise at airspeeds below 120 knots. Above 120 knots airspeed, the test-section broadband background noise was dominated by wind-induced dipole noise (except at lower harmonics of fan blade-passage tones) most likely generated at the microphone or microphone support strut. (Certain tones in the acoustic spectra were probably generated by the microphone support strut.) Third-octave band and narrow-band spectra are presented for several fan operating conditions and test-section airspeeds. The background noise levels compared well with published in-flow background noise from other wind tunnels. The data suggest that background noise levels can be reduced by making improvements to the microphone wind screen or support strut. Empirical equations are presented that related variations of fan noise with fan speed or blade-pitch angle. An empirical expression for typical fan noise spectra is also presented. Fan motor electrical power consumption is related to the noise generation. Preliminary measurements of sound absorption by the test-section lining indicate that the 152-mm thick lining will adequately absorb test-section model noise at frequencies above 300 Hz.</p>			
17. Key Words (Suggested by Author(s)) Wind tunnel noise Flow noise Acoustics Fan noise		18. Distribution Statement Unclassified-Unlimited <p style="text-align: right;">Subject Category – 71</p>	
19. Security Classif. (of this report) Unclassified	20. Security Classif. (of this page) Unclassified	21. No. of pages 43	22. Price A03